INFLUENCE OF MICRODAMAGE HEALING ON STRESS AND DISPLACEMENT FIELDS NEAR A CRACK TIP

A Thesis

by

ABDULLAH MOHAMMED A ALQAHTANI

Submitted to the Office of Graduate and Professional Studies of
Texas A&M University
in partial fulfillment of the requirements for the degree of

MASTER OF SCIENCE

Chair of Committee,	Dallas N. Little
Committee Members,	Robert Lytton
	Anastasia Muliana
Head of Department,	Robin Autenrieth

August 2019

Major Subject: Civil Engineering

ABSTRACT

Asphalt is one of the most common materials in pavement construction in the world. The United States has more than 4.3 million kilometers of roads and highways, with 94 percent of those being flexible pavement according to the National Asphalt Pavement Association. Moreover, the asphalt mixture is a complex material which is a blend of asphalt binder, aggregate, and air voids. The properties of these components have a major impact on the overall performance of the asphalt mixture. Furthermore, asphalt concrete pavement is affected by traffic loading, temperature, moisture, and aging. Pavement deteriorates under the abovementioned conditions; for example, cracking, raveling, and potholes can develop impacting pavement serviceability. Past studies have demonstrated that various asphalt mixtures have the ability to heal with time. Healing can counteract deterioration on asphalt pavements performance. Numerous researchers have proposed several models for predicting healing of microdamage in different materials. However, most of those models were developed to predict the responses under specific states, and consequently, usually do not represent the behavior of material accurately. The main purpose of this research is to study the influence of microdamage healing on stress intensity factor (SIF), displacement, and stress fields near a crack tip in the materials that have the ability to heal. The microdamage healing model that is used in this study considers the effects of both instantaneous healing and time-dependent bonding strength. The results indicate that an increase in the value of bonding strength and the length of the healing process zone lead to a reduction in both stress and displacement fields near the crack tip.

DEDICATION

This thesis is dedicated to my advisor Dr. Dallas N. Little for his

Advice, Guidance, Support and Motivation

throughout my degree path, and for the many others who taught me "each letter."

ACKNOWLEDGEMENTS

First and foremost, I would like to thank my supervisor, Dr. Dallas N. Little for his valuable guidance and advice. He inspired and motivated me to see beyond the limits of my project. His collaborative leadership contributed exceedingly to my work. Without all of his effort, it would have been impossible for me to earn my Master of Science degree.

I would also like to thank Dr. Masoud Darabi for his guidance and assistance throughout this work, as he explained and demonstrated topic related precedents in materials engineering. Moreover, I thank my other advisory committee members, Dr. Robert Lytton and Dr. Anastasia Muliana for their guidance and encouragement.

I am also grateful to the administrators of Texas A&M University (TAMU) for providing me with a beneficial environment, resources and facilities to complete this degree plan.

Last but not least, my beloved family, friends, and colleagues were invaluable for their understanding and support as I completed this work. Without their help, I would have struggled even more while doing this work. Thank you all.

CONTRIBUTORS AND FUNDING SOURCES

This work was supervised by a thesis committee consisting of Dr. Dallas N. Little (advisor) and Dr. Robert Lytton from the Department of Civil Engineering and Dr. Anastasia Muliana from the Department of Mechanical Engineering and Dr. Masoud Darabi from the University of Kansas. All work for the thesis was completed independently by the graduate student.

The graduate student was financially supported by Saudi Arabia government throughout his graduate program.

TABLE OF CONTENTS

Page

Page

LIST OF FIGURES

Page

Page

Page

LIST OF TABLES

Page

1. INTRODUCTION

1.1 Introduction

Asphalt material is one of the most commonly used materials in pavement construction in the world. The United States has more than 4.3 million kilometers of roads and highways, with 94 percent of those being flexible pavement according to the National Asphalt Pavement Association. Moreover, the asphalt mixture is composed of asphalt binder, aggregate, and air voids. The properties of these components have a major impact on the overall performance of the asphalt mixture. Furthermore, asphalt concrete pavement is affected by traffic loading, temperature, moisture, and aging. Pavement deteriorates under abovementioned conditions, and its microstructure changes which results in extensive microdamage (micro cracks and micro voids) especially under severe conditions. Microdamage coalescence causes the mechanical properties of the material to degrade. This process of deterioration can eventually result in structural failure. However, in asphalt material, a process known as healing, an intrinsic property of asphalt, is competing with the deterioration process. Healing restores the original mechanical properties (i.e., strength or stiffness) of the material and increases fatigue life.

Since the turn of the century, numerous experimental studies have shown that polymers, biomaterials, and asphalt binders have the capability to heal and regain some of their mechanical properties in certain circumstances (Kessler and White, 2001; Brown et al., 2002; Reinhardt and Jooss, 2003; Bhasin et al., 2008). In addition to these materials, composite materials are another class of the engineering materials that are apt to heal at high temperatures and during rest periods (Little and Bhasin, 2007; Bhasin et al., 2008; Bhasin et al., 2011).

Many studies have shown that asphalt material is expected to heal and recover some of its mechanical properties during summers and rest periods (Kim and Little, 1990; Lee and Kim, 1998; Little and Bhasin, 2007; Bhasin et al., 2008). During the rest periods, the wetting surfaces of the micro cracks come into contact with each other because of the effect of the surface free energy, and consequently recover some of their bond strength. The wetting surfaces of the micro crack result in partial healing, also known as instantaneous healing (Wool and O'Connor, 1981). Moreover, the damaged material may regain all of its mechanical properties during long rest periods and becomes identical to its initial state (Carpenter and Shen, 2006; Little and Bhasin, 2007). This phenomenon is known as time-dependent healing (Wool and O'Connor, 1981). However, higher loading magnitudes or more loading applications have proven to reduce the ability of the material to heal since regions of greater damage are less likely to heave as a result of a higher gradient of molecular disturbance associated with damage (Little et al., 2001).

Researchers have proposed numerous phenomenological based models and micromechanical based models for predicting microdamage healing in various materials (Wool and O'Connor, 1981; Schapery, 1989; Little and Bhasin, 2007; Bhasin et al., 2007). Wool and O'Connor (1981) proposed a phenomenological based model for crack healing in polymeric material and defined a macroscopic recovery parameter to relate the healing at the micro scale to the variations in the mechanical properties of polymers at the macro scale. Schapery (1989) proposed a fracture mechanics-based model to explain the crack shortening rate for linear viscoelastic materials. However, Schapery (1989) considered only instantaneous healing and assumed it as the total bond strength. Little and Bhasin (2007) built on the work of Wool and O'Connor (1981) and Schapery (1989) and presented a macroscopic recovery parameter to measure healing in asphalt.

The model used in this research combined the effects of both instantaneous healing (short-term) and time-dependent bond strength (long-term). This model mathematically demonstrates the influence of healing of microdamage on the stress intensity factor (SIF), displacement field, and stress field in the vicinity of a crack tip in elastic media. The results of the model in elastic media are transformed into viscoelastic media using the third correspondence principle (CP-III). In fact, constitutive models must consider the healing property of engineering materials, or they underestimate the fatigue life which results in an improper design; modeling healing is critical for more accurate predictions of fatigue life.

1.2 Problem Statement

Since asphalt is the most commonly used material in road construction, it is critical to model microdamage healing to accurately forecast the overall performance. Furthermore, asphalt concrete pavement is subjected to traffic loading, temperature, moisture, and aging. It deteriorates under abovementioned conditions and therefore distress such as cracking, raveling, and potholes can develop.

Numerous experimental studies have shown that polymers, biomaterials, and asphalt binders have the capability to heal during unloading stage and retrieve some of their mechanical properties under particular conditions such as rest periods and high temperatures. Evidence from past studies shows that healing impacts the asphalt mixtures performance. Furthermore, previous studies on asphalt healing have provided first steps to understand the healing process. However, the healing phenomenon is not well understood, and no sophisticated model has yet been developed to predict the influence of healing on microdamage in various materials.

Researchers have mostly concentrated on introducing long rest periods (e.g. 1 hour, 2 hours, 12 hours, and 24 hours) between loading cycles in the fatigue test. However, in reality, the

rest period might be shorter (e.g. in seconds), particularly when a high traffic roadway is considered. To assess healing characteristics during short rest periods, some researchers used an intermittent loading concept in the fatigue test of asphalt binders and mixtures. Furthermore, numerous researchers have proposed several models to evaluate microdamage healing. Unfortunately, many models only indicate responses in limited conditions, resulting in inaccurate prediction of the actual behavior of the material. Therefore, this study aims to appraise the influence of microdamage healing on stress intensity factor (SIF), displacement, and stress fields near the crack tip by considering the effects of instantaneous and time-dependent healing.

1.3 Objective

The main objective of this study is to examine the influence of microdamage healing on SIF, displacement and stress fields near the crack tip. The following objectives also will be achieved:

1. Add to the body of knowledge and discourse about microdamage healing;
2. Describe the influence of the bonding strength and the length of the healing process zone on the displacement and stress fields;
3. Determine the effect of the loading-unloading conditions on the healing process;
4. Evaluate the effect of using distinctive coefficients to delineate the bonding strength and relaxation time;
5. Assess the impact of rest periods on crack shortening.

2. BACKGROUND

2.1 Crack Closure Mechanisms

Elber (1970, 1971) discovered that a crack can close during an experimental study and realized that a fatigue crack can close even at a far field stress. Crack shortening can be affected by several factors such as conditions close to the crack tip, the crack length, and the stress state. Many researchers have looked into the healing process of crack shortening and classified different forms of fatigue crack closure such as the plasticity induced crack closure, roughness induced crack closure, and fluid induced crack closure.

2.2 Crack and Healing in Asphalt

Fatigue cracking is one of the main distresses observed in asphalt concrete (AC) and responsible for the pavement service life reduction. As illustrated in Figure 1, distinctive forms of cracks can be detected from macro to micro scale:

- In the field, cracks observed at the top layer can be either top-down cracks or bottom-up cracks. The top-down cracks develop at the surface of the top layer as a consequence of tensile stress, shear stress, environmental condition and ageing; the bottom-up cracks develop at the bottom of top layer due to horizontal tensile strains.
- In the laboratory, cracks are observed in asphalt samples due to applications of load.

Additionally, cracks can be either cohesive or adhesive. Cohesive cracks take place inside the asphalt binder or mastic (asphalt binder and filler); whereas, the adhesive cracks occur between aggregates and asphalt binder.

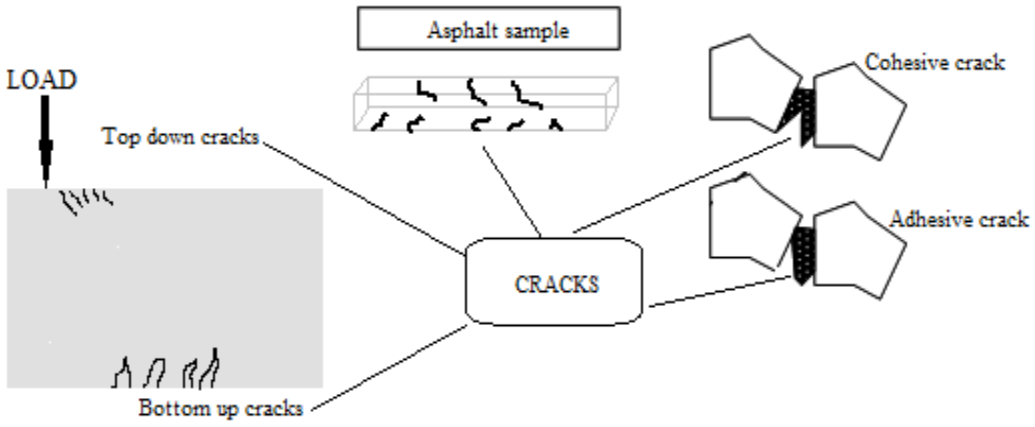

Figure 1 Illustration of distinctive forms of cracks of asphalt materials.

As mentioned previously, asphalt material heals and regains some or all of its strength. Healing is an intrinsic property of asphalt and counters the deterioration process. The healing phenomenon can be observed at multiscale within different modes as follows:

- At macro scale: Healing is believed to occur during rest periods and high temperatures.
- At micro scale: Healing is observed in either the cohesive or the adhesive zones of asphalt mixtures. Healing is defined as cohesive when cross linking of binder at the micro crack face occurs; healing is defined as adhesive when binder and aggregate interface and re-bond.

2.3 Healing in Flexible Pavement Design

Fatigue based mechanistic pavement design approach is used worldwide for the thickness design of AC. In this approach as shown in Figure 2, horizontal tensile strain, calculated at the bottom of asphalt layer (Surface Course), is the main input. The traffic loading, modulus of elasticity (E), Poisson's ratio (ν), and thickness of each layer are the required inputs in this method. The horizontal tensile strain is employed in the fatigue equation for an estimation of load cycles

to failure. If the design number of loads is less than the estimated number of load cycles, a larger thickness is required in order to minimize the strain level and to increase the life of the pavement. Due to the disparity between the fatigue test and the AC fatigue, the experimental results are scaled using the so-called shift factor which can be as high as 20 (Little and Bhasin, 2007). For instance, a shift factor in the Shell Pavement Design Manual (1978) considers the effect of both healing and the traffic lateral wander. The field fatigue life can be calculated with the following equation:

$$N_{FIELD} = N_{LAB} \times H \times V \tag{1}$$

where H is the factor of healing and V is the factor of lateral wander.

Many trials have correlated fatigue damage with the dissipated mechanical energy. For instance, Lytton et al. (1993) proposed another shift factor using the gain in the dissipated energy of a load series after a rest period. The field fatigue life can be determined with the following formula:

$$N_{FIELD} = N_{LAB} \times SF_h \times SF_r \times SF_d \tag{2}$$

where shift factors are: SF_h caused by healing; SF_r caused by residual stresses; and SF_d caused by resilient dilation.

The equation for the healing shift factor has been found to be:

$$SF_h = 1 + a(t_r)^b \tag{3}$$

where t_r is the rest period in seconds, a is the healing coefficient, and b is the healing exponent.

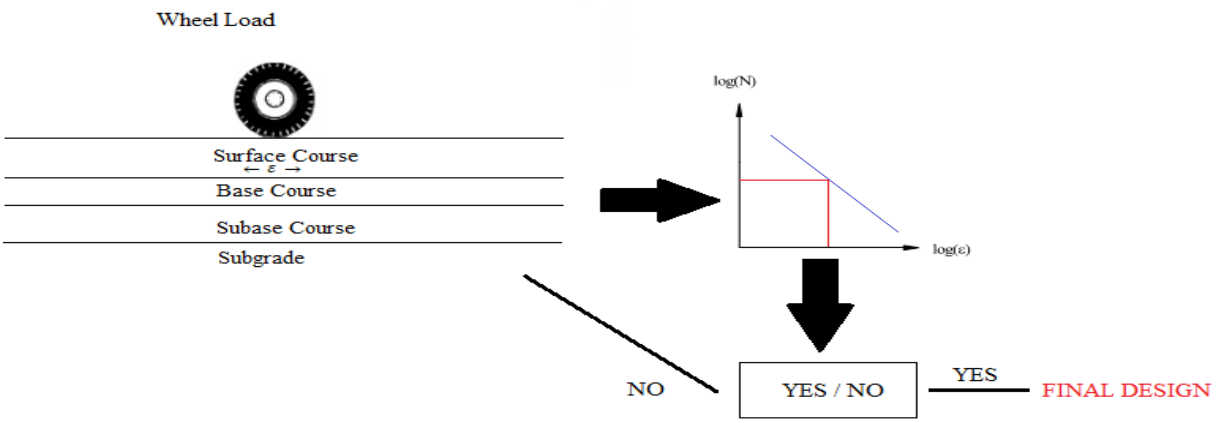

Figure 2 Fatigue based thickness design approach.

Little et al. (2001) implemented the healing potential of asphalt binder in order to improve the shift factor concept:

$$\frac{dh}{dN} = Function\left(t_r, h_1, h_2, h_\beta\right) \tag{4}$$

where $\frac{dh}{dN}$ is the healing rate per load cycle which is the same concept as crack rate per load cycle$\left(\frac{dC}{dN}\right)$ in fracture mechanics, $h_1$and h_2 are the short-term and long-term healing rates, respectively, and h_β is the maximum healing value in asphalt.

In fact, there is no unique value and many distinctive shift factors are used. Also, shift factors proposed by several investigators vary; for example, the shift factors proposed by Nottingham University vary between 77 and 400. The shift factors are dependent on various factors such as test types, experimental conditions, loading modes in the laboratory and the field. Other examples of shift factors proposed by several investigators are listed in Table 1.

Table 1 Fatigue Shift factors (SF) in the United States (U.S.) and United Kingdom (U.K.)

Country	Organization	Healing	Crack propagation	Traffic wander	Total
U.S.	Asphalt Institute				13
U.S.	SHRP A-003				10-13
U.K.	Nottingham Pell	5	20	1	100
U.K.	Nottingham Brown	20	20	1.1	440
U.K.	Shell SPDM 1978	5	1	2	10

Schapery (1984, 1988) proposed an equation to obtain the fracture speed and healing speed. The difference between them is known as the crack growth speed. Little et al. (1997) proposed an alternative equation, Eq. (5), for healing speed by analogy with the theory of rate process, consistent with Schapery's fracture theory:

$$\dot{C_h} = \left(\frac{k_h E_R D_{1c} J_R}{2\tau_h}\right)^{\frac{1}{m_c}} \beta \tag{5}$$

where $\dot{C_h}$ is a healing speed, k_h is a function of m_c equal to 1/3, E_R pseudo strain reference modulus, D_{1c} is a compressive creep compliance coefficient, J_R is rate of change of dissipated pseudo strain energy per unit of newly formed crack area, τ_h is healing surface energy, m_c is a slope of compressive curve of compliance versus time on the logarithm scale, and β is length of the bonding zone or the length of the healing process zone.

Little et al. (2001) used hyperbolic form of the following equation, Eq. (6), to analyze the asphalt healing test data:

$$\dot{h} = \dot{h}_2 + \frac{\dot{h}_1 - \dot{h}_2}{1 + \left(\frac{\dot{h}_1 - \dot{h}_2}{h_\beta}\right) t_r} \tag{6}$$

where $\dot{h}_1$ is an initial healing rate, $\dot{h}_2$ is a final healing rate, h_β is a maximum healing index increase, and t_r is a rest period between applications of load.

2.4 Characterization of Healing of Asphalt Materials

Developing a model for characterizing the healing process is critical to predict the damage caused in AC with a high degree of accuracy, but it requires expensive and time-consuming laboratory tests. Also, some researchers have studied the healing process by focusing on a variety of binders, mastic (binder and filler), mortar (binder, filler, and fine aggregate), asphalt mixture and the asphalt pavement structure. The common method to investigate the changes in materials properties is to induce rest periods between the load applications and then compare between the properties with and without rest periods. Unfortunately, the results depend on the experimental methods and conditions limiting usage in computational modeling. Fatigue related healing tests (FH) and fracture related healing tests (FRAH) are the common laboratory tests used to characterize healing ability of asphalt materials. FH are also divided into two categories which are fatigue related healing with intermittent loading (FHI) and fatigue related healing with storage periods (FHS). The intermittent loading is applied in the FHI test, while a continuous loading with an inserted storage period is considered in the FHS tests. The rest period is applied between two fracture tests in the FRAH. Table 2 summarizes some more commonly used methods for asphalt healing characteristics.

Table 2 Tests to characterize the healing of asphalt materials

		Asphalt Binder, Mastic, and Mortar	**Asphalt Mixture**	**Asphalt Structure**
Fatigue related healing tests (FH)	Fatigue related healing with intermittent loading (FHI)	Dynamic Shear Rheometer (DSR) Dynamic Mechanical Analysis (DMA)	Two-Point Bending Test Three-Point Bending Test Four-Point Bending Test Uniaxial Push Pull	
	Fatigue related healing with storage periods (FHS)	DSR	Indirect Tension Test Two-Point Bending Test Four-Point Bending Test	
Fracture related healing tests (FRAH)		DSR and DMA	Uniaxial Tension Test Flexural Test	
In situ test				Falling Weight Deflectometer (FWD) Stress Waves
Other methods		Scanning Electron Microscopy (SEM) Surface Energy		

The next three sections focus on the healing of asphalt binder, asphalt mixture, and asphalt structure based on some of these tests.

2.5 Research on Healing of Asphalt Binder and Mastic

Asphalt binder is crucial in countering fatigue cracking damage, consequently, asphalt binder has been studied by researchers. Investigators have evaluated the nature of fatigue in asphalt binder and recognized that fatigue tests underestimated the actual fatigue life resulting from rest periods between load applications on asphalt concrete pavement. Some investigators applied intermittent loading and discovered that asphalt binder has the ability to heal. Inspired by the work of Wool and O'Connor (1981) on crack healing of polymeric materials, Bhasin et al. (2009) defined three stages of asphalt binder healing: (1) wetting of both surfaces of a nano crack; (2) interfacial cohesion between the surfaces of crack, which causes immediate strengthening; and (3) diffusion and randomization of molecules between the crack surfaces, which causes long-term strengthening.

Kim et al. (1991) examined the healing properties of binder samples with scanning electron microscopy (SEM). The binder samples were composed of Ottawa sand including 13% (by mass) asphalt binder. The Izod impact test machine was used after curing in order to split the samples. Then the surfaces of the split samples were reconnected to each other. The test data indicated that there are two stages in the healing mechanism: interpenetration and bonding. Kim et al. (1991) found that the interface disappeared over time when the two pieces of binder reconnected. Over time, the bonding energy developed and strengthened the healing of the binder.

Elphingstone (1997) computed the surface energy of the binder using the dynamic Wilhelmy plate method. Lytton (2000) defined surface free energy in two ways: the Lifshitz –Van der Waals component, and the Lewis acid–base component. Lytton et al. (1998) demonstrated that the non-polar surface energy decreases when the rate of short-term increases; conversely, the polar acid-base surface energy decreases if the rate of long-term increases. Moreover, Lytton (2000)

described the Lifshitz –Van der Waals component as having a negative impact on short-term healing, and the Lewis acid-base component as having a positive impact on long-term healing.

By measuring the surface energy, Little et al. (1999) explored the mechanisms of fracture and healing of asphalt mixtures. The test results illustrate a corresponding link between the healing potential and acid-base surface energy, and an inverted link between the healing potential and Lifshitz -Van der Waals surface energy.

Kim et al. (2002) conducted dynamic mechanical analysis (DMA) test under controlled-strain mode to investigate fatigue damage and healing in asphalt mixtures and sand asphalt samples. To estimate the effect of rest periods in healing, they used a pseudo stiffness parameter.

Kim et al. (2003) performed strain-controlled torsional tests at the following strain levels: 0.20; 0.28; and 0.40%. Hysteretic stress-strain behavior due to cyclic loading is shown in Figure 3 at two different cycles, the 80th and 3,000th. The slope of stress-pseudo strain response at the 3000th cycle is smaller than at the 80th cycle, which indicates that the microdamage has occurred. Their study also revealed that a rest period before major damage occurs results in a greater healing effect.

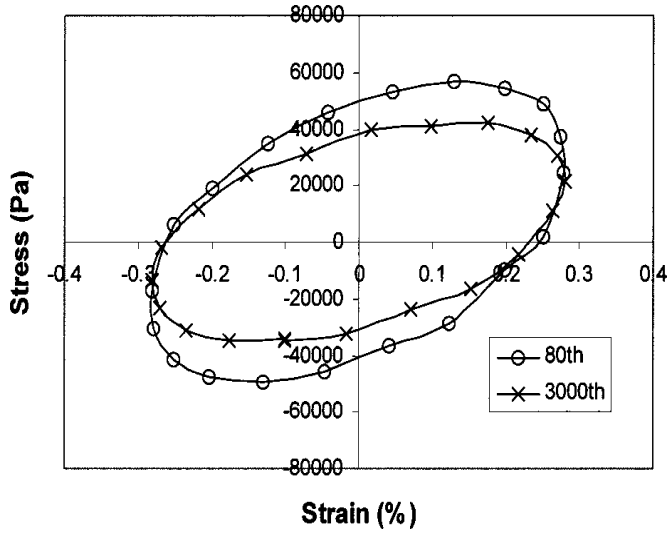

Figure 3 Stress-strain hysteresis loops (Kim et al., 2003).

Kim et al. (2003) employed the torsional shear cyclic tests at 0.28% strain (with ten two-minute rest periods) to investigate the effect of microdamage healing. Figure 4 shows the impacts of microdamage healing as a result of rest periods. The results indicate an increase in fatigue life due to the rest periods. Also, the investigators found that the dynamic modulus increases after the introduction of a rest period causing an increase in fatigue life.

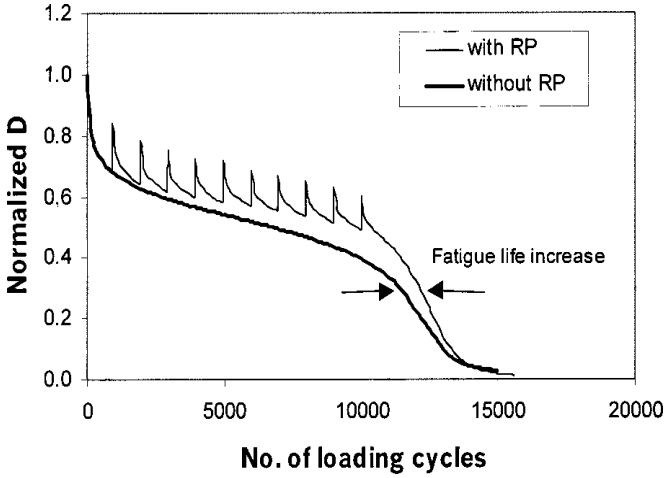

Figure 4 Normalized dynamic modulus versus number of loading cycles with and without rest periods (Kim et al., 2003).

Maillard et al. (2004) performed tensile tests on bitumen films held between steel spheres to mimic bitumen bound by aggregates. The transmitting ultrasonic waves were used to measure the healing rate in the bitumen film. The resulting damage in the bitumen film decreased the amplitude of the ultrasonic signal; whereas, the amplitude of the ultrasonic signal increased due to the healing process after applying a tensile load.

Kim et al. (2006) measured the healing characteristics of binders in distinctive asphalt mixes based on the retrieved dissipated creep strain energy per unit of time. They found that because the hysteresis loop contains both irreversible and reversible dissipated energy, measurements adjacent to the hysteresis loop during the cyclic loading test would not be reliably

accurate. However, only the irreversible dissipated energy is instrumental in causing damage. The authors used the rheological parameters obtained from the creep test to find irreversible dissipated energy.

Shen et al. (2007) applied intermittent loadings in the fatigue test of asphalt binders to evaluate the healing under short rest time period. They stated that the short rest period increases fatigue life and the endurance limit of some mixtures.

Shen et al. (2010) investigated the effect of cohesive healing on different binder types without considering the aggregate interaction. They performed a dynamic shear rheometer (DSR) test on two different types of asphalt binder PG64-28 (neat binder) and PG70-28 (polymer modified binder) under two temperatures conditions (15 ºC and 25 ºC) and 10 Hz frequency, with constant stress mode and with different rest periods to determine the effect of cohesive healing. Also, in this study the original binder without an aging effect was used to determine the factors influencing the healing process. The complex shear modulus (G^*) is used to represent the material performance deterioration as a result of cyclic loading since the results of neat binder indicate that fatigue damage does not affect the phase angle. As seen in Figure 5, an increase in the short rest periods leads to a reduction in the G^* value in longer loading cycles. The authors stated that increasing rest periods enhanced the healing effect. This study also revealed that several factors such as type of binder, temperature, and aging can affect the healing rate.

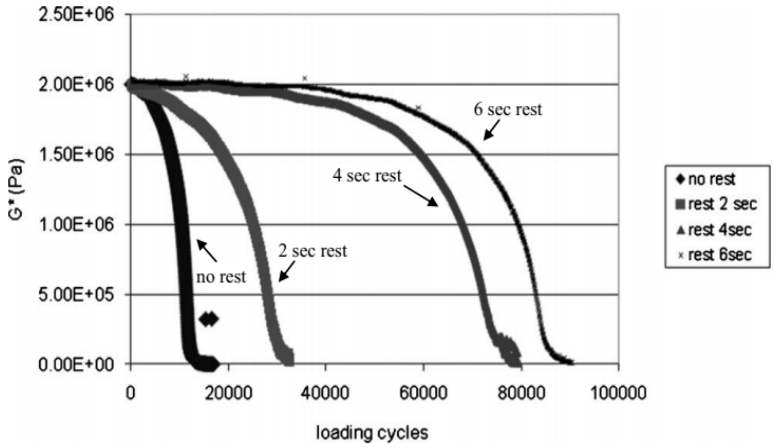

Figure 5 G* deterioration curve for the neat binder with different rest periods (Shen et al., 2010).

2.6 Research on Healing of Asphalt Mixture

Several researchers evaluated healing properties using intermittent loading with long rest periods (Bonnaure et al., 1982; Kim et al., 1997; Little et al., 2001). Recovery of modulus and extension of fatigue life after rest periods are used to assess healing impact. However, this approach is not indicative of field conditions because there are long and short rest periods between load applications.

Bonnaure et al. (1982) explored how the rest period affects fatigue life by using intermittent loading. In the three-point bending tests, rectangular beams (230mm x 30mm x 20mm) were tested under both controlled stress and controlled strain loading conditions, three temperatures (5°C, 20°C, and 25°C), several rest periods (0, 3, 5, 10 and 25), and 40 Hz loading frequency. According to the results, rest periods have a positive impact on healing.

Relaxation is the only occurrence during the period of rest, according to Kim et al. (1990). Also, the corresponding principal theory suggests that if rest periods are included in the loading history, the stress prior to the rest period must be equal or less than the stress following the rest

period for the same pseudo strain. They found that the chemical healing mechanism increased the stress after the rest period.

Kim et al. (1990) performed several tests (e.g. uniaxial tests; relaxation test; and a constant strain rate simple loading test with rest periods) to study the healing mechanism. The uniaxial test results disclosed the fracture healing of bituminous material. The nonlinear viscoelastic correspondence principle was used to explain the time dependent effect of relaxation and to measure the chemical healing.

Little et al. (2001) conducted a flexural beam bending test with long rest periods (24-hours). The tests results indicate that the fatigue life can be improved more than 100-fold based on the bitumen type.

Planche et al. (2004) continuously loaded asphalt specimens, and then inserted rest periods of 40 minutes or six hours; the response of the material was measured before and after the rest periods. They found that material response is affected by rest periods, particularly when they are inserted before failure.

Carpenter et al. (2003, 2006, and 2007) studied the healing capability of AC based on energy principles by performing the four-point bending tests. The results show that the Plateau Value (PV) is decreasing when the rest period increases from 0 to 9 seconds which corresponds to an extended fatigue life.

2.7 Research on Healing of Asphalt Concrete

The healing property of asphalt materials is a recognized fact which can lead to increase the service life of flexible pavement. As mentioned previously, two methods used to study the healing of asphalt material are experiments and computational modeling based on viscoelasticity theories.

Groenendijk (1998) performed the Falling Weight Deflectometer (FWD) and analyzed measurements during accelerated pavement testing. The weekend (Friday afternoon to Monday) was assumed to be the rest period and continuous load repetitions were applied during the weekdays. The FWD is performed before and after the rest period. As seen in Figure 6, the data on Monday is higher than the data on Friday which indicates AC stiffness increases during rest demonstrating that healing has occurred.

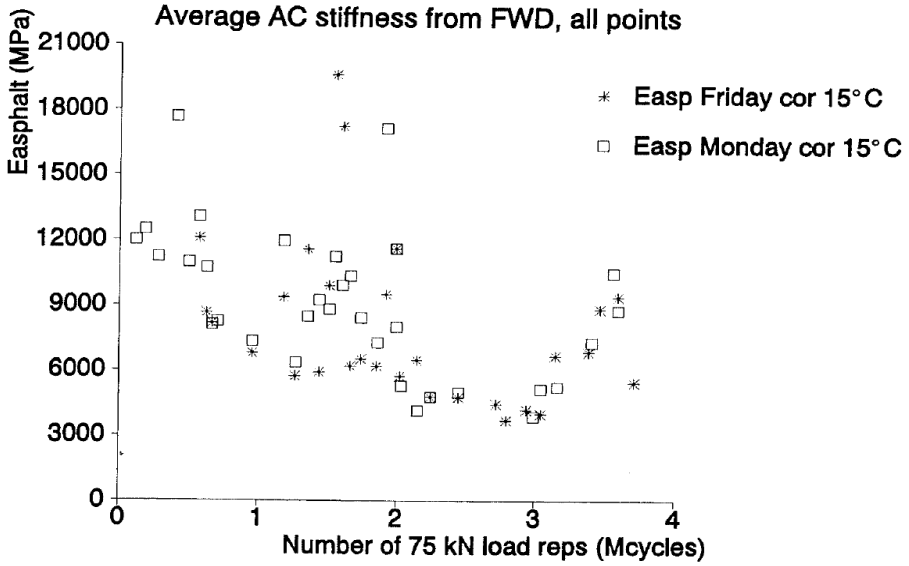

Figure 6 Change of back-calculated stiffness of asphalt concrete due to rest periods (Groenendijk, 1998).

Williams at el. (2001) performed a surface wave tests (nondestructive test) in order to identify the healing abilities of AC; they conducted tests at the accelerated pavement testing facility at FHWA Turner-Fairbank Highway research center. The results show an increase modulus of elasticity of AC, which is believed to be a result of microdamage healing.

2.8 Macroscopic Recovery Parameter for Describing Healing

De Gennes (1971) developed a model known as reptation model (Tube model) in order to describe the tangled chain motions in a bulk material. Several researchers have used this model to study the healing of crack in a polymer material (Prager and Tirrell, 1981; Wool and O'Connor, 1981). Wool and O'Connor (1981) modified the reptation model in order to ascertain the time needed for healing due to the molecules inter diffusion between crack surfaces. The authors divided the crack healing process in polymer into five stages, namely, (a) surface rearrangement, (b) surface approach, (c) wetting, (d) diffusion, and (e) randomization. These healing stages are shown in Figure 7.

The fracture stress σ is used to measure the stress transmitted across the crack plane. In steps (a) and (b), the fracture stress is greater than or equal to zero, whereas the fracture stress in step (c) is equal to the stress as a result of wetting or surface attraction. Also, the fracture stress in step (d) is the sum of the stress due to wetting σ_0 and the stress due to diffusing σ_d. In the last stage, the fracture stress has the same value as the fracture strength of the virgin material.

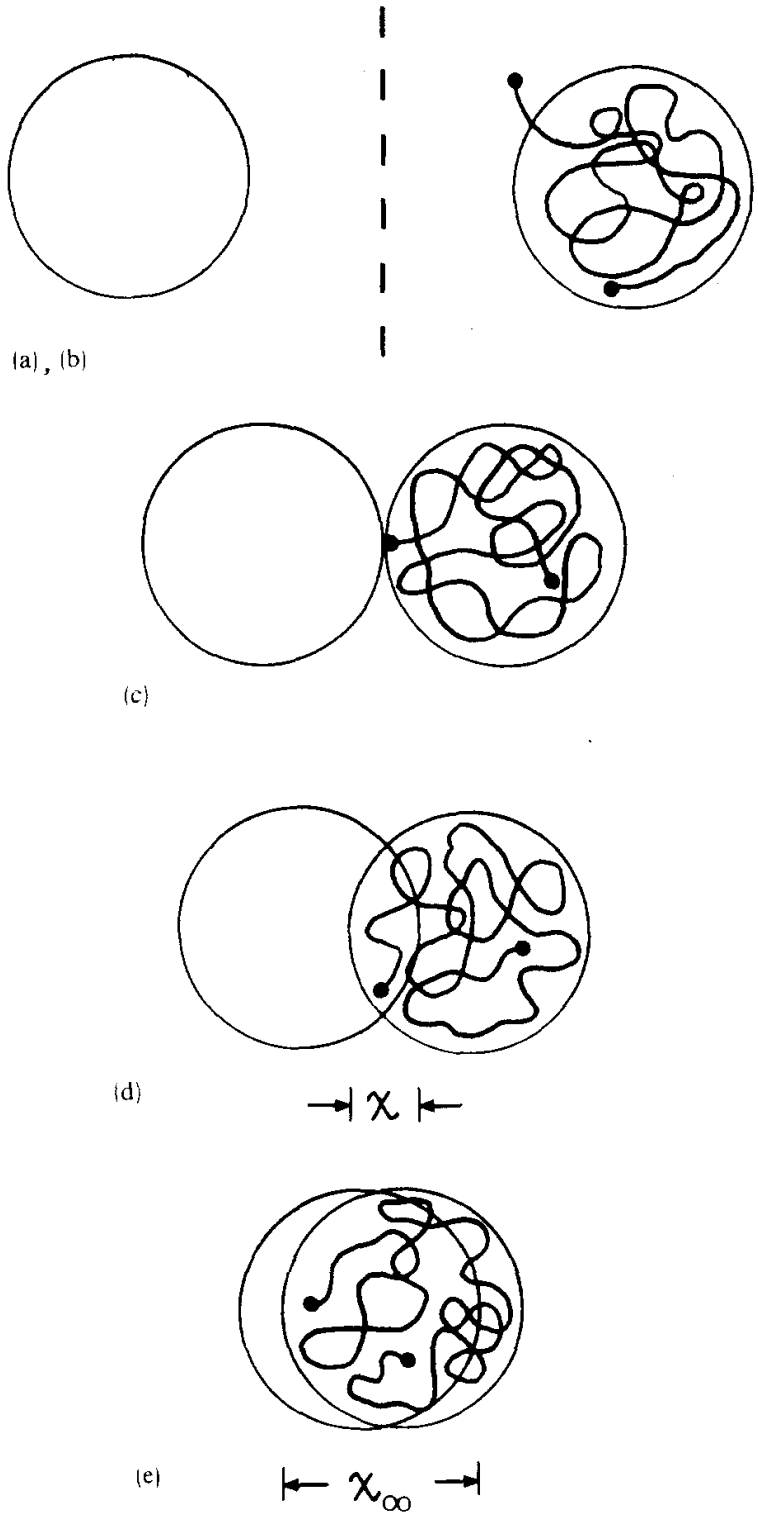

Figure 7 Schematic diagram showing the five stages of crack healing for two random-coil chains on opposite crack surfaces (Wool and O'Conner, 1981).

Wool and O'Connor (1981) proposed a convolution integral in order to explain macroscopic recovery R in a polymeric material by considering the material intrinsic healing function and a wetting distribution function:

$$R = \int_{-\infty}^{t} R_h(t-\tau)\frac{d\emptyset(\tau, X)}{d\tau}\,d\tau \tag{7}$$

where $R_h(t-\tau)$ is the intrinsic healing function, $\emptyset(\tau, X)$ is the wetting distribution function, X is a domain in the interface of crack, t is the time, and τ is the running variable on the time axis.

Under the following conditions, the macroscopic recovery or healing function, Eq. (7), can be reduced to the intrinsic function:

$$\dot{\emptyset}(t) = \delta(t) \tag{8}$$

where $\delta(t)$ is the Dirac delta function.

The diffusion of chain ends at some time of healing process may be delayed or prevented as a result of chemical reaction and rearrangement of surface. Therefore, in order to solve this problem, a diffusion initiation function $\psi(t)$ such that σ_d is obtained as:

$$\sigma_d = Kt^{0.25} * \psi(t) \tag{9}$$

where the asterisk indicates convolution. Once all the required chain ends are accessible for immediate reptation across the interface, then $\psi(t) = \delta(t)$, and

$$\sigma_d = Kt^{0.25} \tag{10}$$

where K is a constant depends on temperature T, pressure P, and molecular weight M.

The intrinsic healing function represents the strength increase as a result of interfacial cohesion and inter diffusion of molecules between the crack surfaces. Wool and O'Conner (1981) revealed that the intrinsic healing function for polymer can be denoted with the following equation:

$$R_h(t) = R_0 + Kt^{0.25} \bullet \zeta(t) \tag{11}$$

where the • implies convolution and $\zeta(t)$ is the molecules surface arrangement. This model was proposed for a simple polymer with short-term healing as a result it is not valid for the asphalt materials. Also, they stated that the exponent varies from 0.25 to 0.5 for long duration.

Wool and O'Conner (1982) explained the intrinsic healing function for stress, strain, and energy as follows:

$$R_h(\sigma, t) = \frac{\sigma_0 + Kt^{0.25}}{\sigma_\infty} \tag{12}$$

$$R_h(\varepsilon, t) = \frac{\varepsilon_0 + Jt^{0.25}}{\varepsilon_\infty} \tag{13}$$

$$R_h(E, t) = \frac{(\sigma_0 + Kt^{0.25})^2}{2YE_\infty} \tag{14}$$

where subscript ∞ stand for the virgin or healed state, ε_0 is a fracture strain recovery as a result of wetting, J is a constant equal to $\frac{K}{Y}$ where Y is a tensile modulus, and E is a fracture energy given by $E = \frac{\sigma^2}{2Y}$.

Bhasin et al. (2008) used a sigmoid function in order to represent time dependent healing in asphalt material as a result of interdiffusion of molecules between the crack faces. The formula of the healing function that was used follows:

$$R_h(t) = R_0 + p\left(1 - e^{-qt^r}\right) \tag{15}$$

where $R_h(t)$ is a time-dependent function that shows the increase in a mechanical property of the wetted crack surfaces, R_0 shows the effect of instantaneous healing as a result of cohesion at the interface of crack, and the parameters, $p, q,$ and r represent the effect of healing as a result of the

interdiffusion of molecules between the surfaces of crack. They performed DSR test to obtain these parameters for three different types of asphalt.

The wetting distribution function is employed to represent a wetting of crack surfaces. Schapery (1989) proposed an equation to show the relationship between the cohesion work and the properties of material associated with the wetting of crack faces. Bhasin et al. (2008) proposed the following wetting distribution function using the rate of crack shortening formulation developed by Schapery (1989) and macroscopic recovery concept developed by Wool and O'Connor (1981).

$$\frac{d\Phi(t,X)}{dt} = \dot{a}_b = \beta\left[\frac{1}{D_1 k_m}\left\{\frac{\pi W_c}{4(1-v^2)\sigma_b^2\beta} - D_0\right\}\right]^{\frac{-1}{m}} \tag{16}$$

where W_c is the work of cohesion, $D_0, D_1,$ and m are the parameters of creep compliance, and k_m is a constant. The wetting distribution function in the above equation indicates wetting that happens at a constant rate.

When two pieces of similar mass polymer or bulk polymer contact each other at temperature above the glass transition T_g, the interface slowly shrinks and the strength at interface grows due to the healing of crack. This healing of the crack occurs mainly as a result of the chain diffusion across the interface. The diffusion of chain across the interface is a unique type of mass transfer, which cannot be attributed to the equation of convolution diffusion. As mentioned previously, Wool and O'Connor (1981) investigated crack healing in polymeric materials in terms of five stages. At the end of the second stage, potential barriers related to the inhomogeneities at the interface disappear and chains can move freely across the interface in fourth and fifth stages. The diffusion and randomization stages are most significant since the strength of a material appears in these phases.

Application of the reptation model requires many assumptions about crack healing in polymeric materials. Therefore, the minor chains concept was proposed by Kim and Wool (1983). The motion of a polymer chain is restricted by the other chains. The reptation model is appropriate for describing this phenomenon. Figure 8 shows chain conformations at distinctive time. As it can be seen, the initial tube defined at $t = 0$ is indicated by dashed line at different times. The end part of the chain escapes from the initial tube at $t = t_1$. The part of the chain outside the initial tube grows with time and is known as a minor chain. The memory of the minor chain lost is illustrated at times t_2 and t_3. The first conformations are supplanted by new conformations since the length of the minor chain enlarges with time. The time scale of significance in the problem of a crack healing is in the area of $T_e < t < T_r$. The diffusion and randomization stages are completed by the time $t \approx T_r$ and the healing process is mostly as a result of these stages.

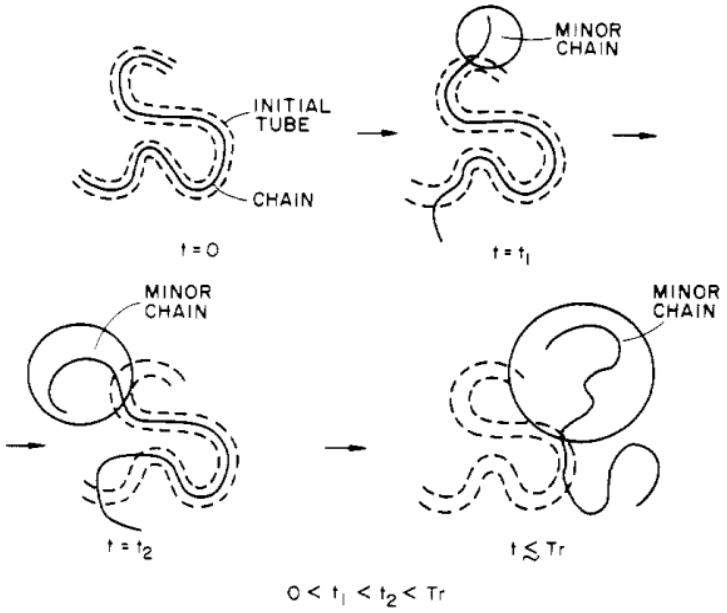

Figure 8 Disengagement of a chain from its initial tube. The emergence and growth of minor chains are also shown. T_r is the tube renewal time (Kim and Wool ,1983).

2.9 Healing Index

A healing index is used in order to assess the healing capability of binder and identify the factors of healing. Distinctive indices have been proposed by researchers, for instance, Tan et al. (2012), proposed two indices, (HI^1 and HI^2) as shown in Eqs. (17) and (18) to explain the healing performance of binder.

$$HI^1 = \frac{|G^*|_{after}}{|G^*|_{initial}} \times 100 \tag{17}$$

where HI^1 is the healing index computed by the ratio of the modulus value, ${G^*}_{initial}$ and ${G^*}_{after}$ are the initial modulus value before and after rest, respectively.

$$HI^2 = \left(\frac{|G^*|_{terminal}}{|G^*|_{initial}}\right)\frac{\left(N_{after} - N_{befor}\right)}{N_{befor}} \times 100 \tag{18}$$

where HI^2 is the healing index computed by the ratio of cycle number, $|G^*|_{terminal}$ is the dynamic modulus value when the cyclic loading stops, N_{before} represents the number of loading cycles before rest, and N_{after} is the number of loading cycles the rest period.

As seen in Figure 9, the response of the material can be greatly affected by the rest periods, particularly if rest periods are applied before failure. Also, it is worth mentioning that the healing capability of asphalt binder aids the modulus recovery and increases the asphalt binder fatigue life.

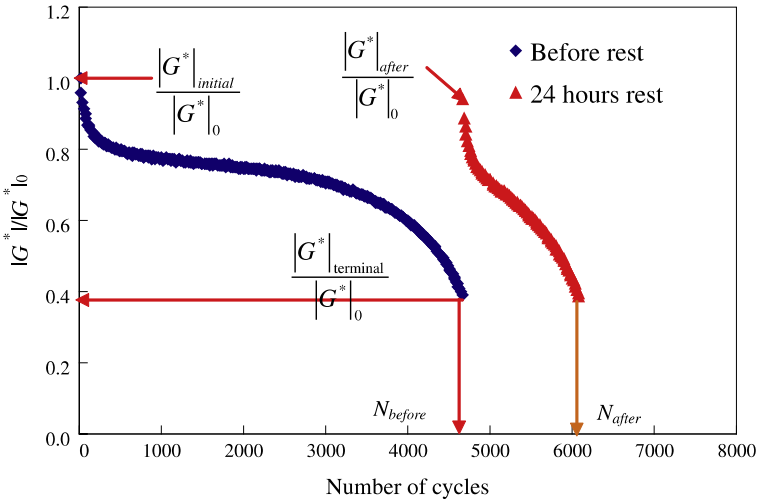

Figure 9 Schematic of fatigue indices (Tan et al., 2012).

2.10 Factors that Influence Healing of Asphalt Materials

Healing in asphalt materials can be affected by several internal and external factors that are listed in Table 3.

Table 3 The factors affecting the rate of healing of asphalt mixtures

Factors Affecting Healing		
Properties of Binder	**Asphalt Mixture Compositions**	**Environments**
Chemical compositions	Binder content	Loading history
Viscoelastic properties	Aggregate structure	Rest period
Surface free energy	Gradation	Temperature
Diffusion	Thickness	Moisture
Modifiers		
Aging		

3. FRACTURE MECHANICS

Every structure requires accurate failure criterion to estimate its failure strength. The common design method does not consider the existence of cracks caused by defects due to manufacturing and handling processes. The existence of cracks leads to a redistribution of stress and stress concentration in the proximity of the cracks and disjointed parts. Therefore, prediction of failure strength using strength criterion might not be consistent. Researchers use fracture mechanics approaches to measure the strength reduction in material containing cracks.

3.1 Linear Elastic Fracture Mechanics (LEFM)

3.1.1 Energy Criterion

Griffith (1921) initially investigated crack nucleation and growth using fracture mechanics and proposed the energy criterion for fracture. He stated that a brittle body fails due to the existence of many internal cracks or flaws which generate local stress concentration. Griffith criterion for crack growth can be expressed as follows:

$$\frac{dU}{da} = \frac{dW}{da} \tag{19}$$

where a is the crack length, U is the elastic energy, and W is the energy require for crack formation. The left-hand side of Eq. (19) states the crack resistance R, and the right-hand side is the elastic energy release rate G (Broek, 1986).

For a crack of length $2a$ in an infinite plate subject to load P as shown in Figure 10. The work done by the load is Pdv where dv is the variation in displacement. Therefore, elastic energy can be computed under the assumption of the linear elastic relation between displacement and loading $v = CP$ as follows:

$$U = \frac{1}{2} CP^2 \tag{20}$$

Substituting this equation into Eq. (19), the energy release rate can be obtained as follows:

$$G = \frac{1}{2B} P^2 \frac{\partial C}{\partial a} \tag{21}$$

where B is the thickness of the plate.

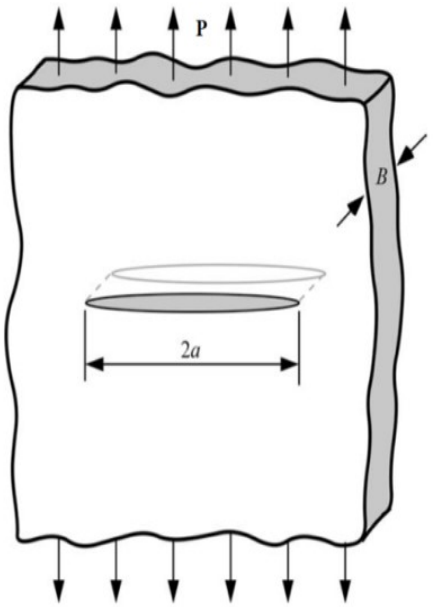

Figure 10 An internal crack in an infinite plate subject to load.

The Griffith criterion assumes that there is no plastic deformation in the material. However, plastic deformation always occurs in many materials.

3.1.2 Stress Intensity Factor Criterion

The stresses distribution in front of a crack tip σ_{ij} as illustrated in Figure 11 can be expressed as follows:

$$\sigma_{ij} = \frac{K_I}{\sqrt{2\pi x}} + f_{ij}(\theta) \tag{22}$$

where subscript *I* pertains to the first mode of fracture, K_I is the stress intensity factor, and x is the distance from the crack tip (Broek,1986). In general, stress intensity factor depends on the applied load, the length of crack, and the specimen geometry. The stress intensity factor for opening mode (Mode-I) is expressed in the following form:

$$K_I = \sigma \sqrt{2\pi a}\ F\left(\frac{a}{b}\right) \tag{23}$$

where σ is the nominal stress and *F(a/b)* is a geometry correction factor.

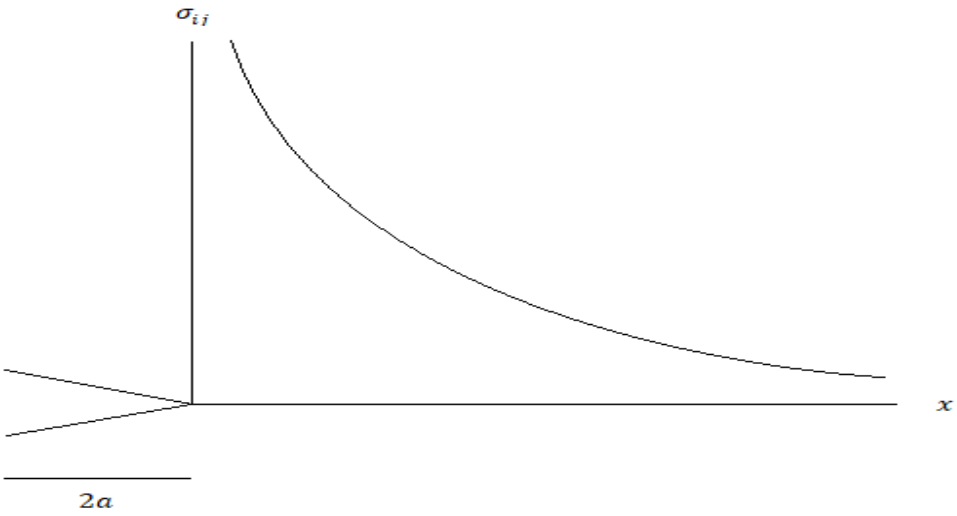

Figure 11 Stress σ_{ij} at the crack tip.

The following equations present the relations between the stress intensity factor K_I and the elastic energy release rate G_I for plane stress and plane strain conditions, respectively:

$$K_I = \sqrt{EG_I} \tag{24}$$

$$K_I = \sqrt{\frac{EG_I}{1-v^2}} \tag{25}$$

3.2 Stress and Displacement Fields

Numerous researchers have studied the stress distributions in the neighborhood of the cracks (Inglis, 1913; Griffith, 1921; Westergaard, 1934). One solution is to introduce an unknown parameter, the Airy stress function $\emptyset$, and check if stress function satisfies equilibrium equations and boundary condition (Williams, 1957; Williams, 1959). Stress field is expressed in Eq. (26):

$$\sigma_{11} = \emptyset_{,22} \; ; \; \sigma_{22} = \emptyset_{,11} \; ; \; \sigma_{12} = -\emptyset_{,12} \tag{26}$$

Stress values found from the above equation already satisfy the equilibrium equations. The stress function must satisfy the biharmonic equation, Eq. (27), in order to satisfy the compatibility equations.

$$\frac{\partial^4 \emptyset}{\partial x^4} + 2\frac{\partial^4 \emptyset}{\partial x^2 \partial y^2} + \frac{\partial^4 \emptyset}{\partial y^4} = 0 \tag{27}$$

and is abbreviated $\nabla^4 \emptyset = 0$. Finally, the boundary conditions of the crack are used to obtain the stress function. The displacement field is the integral form of strain. Regrettably, this technique is complicated as a result of the complicated mathematics. On the other hand, some investigators used the complex variable method to compute the stress field proximal to the crack tip (Hellan, 1985; Sedov, 1972).

Westergard (1939) described the stress and displacement fields near the crack using the complex variable method as follows:

$$\sigma_{11} = Re\ \emptyset' - y\ Im\emptyset'' \tag{28}$$

$$\sigma_{22} = Re\ \emptyset' + y\ Im\emptyset'' \tag{29}$$

$$\sigma_{12} = -y\ Re\ \emptyset'' \tag{30}$$

$$u_1 = \frac{1}{2G}\left(\frac{k-1}{2} Re\emptyset\ - y\ Im\emptyset'\right) \tag{31}$$

$$u_2 = \frac{1}{2G}\left(\frac{k+1}{2} Im\emptyset - y\ Re\ \emptyset'\right) \tag{32}$$

where $k = 3 - 4v$ for plane strain and $k = \frac{(3\ -\ v)}{(1+v)}$ for plane stress. Re is the real part of the complex number, and Im is the imaginary part of the complex number.

The derivative of stress function $\emptyset'$ in the opening mode (Mode-I) can be obtained by using the following equation developed by Sedov (1972).

$$\phi'_{\mathrm{I}} = \frac{1}{\pi\sqrt{\mathrm{z}^2 - \mathrm{a}^2}} \int_{-a}^{a} \frac{\mathrm{g}_2(\xi)\sqrt{\mathrm{a}^2 - \mathrm{z}^2}}{\mathrm{z} - \xi}\ \mathrm{d}\xi \tag{33}$$

where g_2 is the traction loading on the crack surface in the y direction. The stress and displacement fields are calculated in the vicinity of the crack, therefore, the coordinate $y = 0$ is assumed in the calculations. Eqs. (29) and (32) reduce to Eqs. (34) and (35), respectively.

$$\sigma_{22} = Re\ \emptyset' \tag{34}$$

$$u_2 = \frac{1}{2G}\left(\frac{k+1}{2} Im\emptyset\right) \tag{35}$$

3.3 Linear Viscoelasticity

3.3.1 Superposition Principle

The superposition principle or Boltzmann's superposition principle state that the sum of the response (i.e. strain) outputs resulting from individually input (i.e. stress) component is the same as the response resulting from the combined input (Findley et al., 1989).

If a constant stress σ_1 is applied at $t = \xi_1$ then $\sigma(t) = \sigma_1 H(t - \xi_1)$ and the response will be as follows:

$$\varepsilon(t) = \sigma_1 D(t - \xi_1) H(t - \xi_1) \tag{36}$$

where $D(t)$ is the creep compliance and $H(t)$ is the Heaviside function.

If an arbitrary stress $\sigma(t)$ is applied instead of a constant stress, then the sum of a series of a constant stress input can be used to approximate the arbitrary stress as follows:

$$\sigma(t) = \sum_{i=1}^{r} \sigma_i H(t - \xi_i) \tag{37}$$

The strain output under arbitrary stress $\sigma(t)$ will be as follows:

$$\varepsilon(t) = \sum_{i=1}^{r} \Delta\sigma_i D(t - \xi_1) H(t - \xi_1) \tag{38}$$

The Stieltjes integral can be used in order to obtain the strain output, if the number of steps tends to infinity:

$$\varepsilon(t) = \int_{o}^{t} D(t - \xi_1) H(t - \xi_1) \mathrm{d}[\sigma(\xi)] \tag{39}$$

Since the dummy variable ξ is always less than or equal to t, consequently the Heaviside function is always equal to one. Thus Eq. (39) reduces as follows:

$$\varepsilon(t) = \int_o^t D(t-\tau)\frac{\partial\sigma(\tau)}{\partial\tau}\partial\tau \tag{40}$$

If an arbitrary strain $\varepsilon(t)$ is applied, then the stress output under variable strain equals:

$$\sigma(t) = \int_o^t E(t-\tau)\frac{\partial\varepsilon(\tau)}{\partial\tau}\partial\tau \tag{41}$$

where $E(t)$ is the relaxation modulus.

Employing the Laplace transform (LT) to Eqs. (40) and (41) the relation between creep compliance $D(t)$ and the relaxation modulus $E(t)$ as follows:

$$\int_o^t E(t-\tau)\frac{\mathrm{d}D}{\partial\tau}\partial\tau = \int_o^t D(t-\tau)\frac{\mathrm{d}E}{\partial\tau}\partial\tau = 1 \tag{42}$$

3.3.2 Correspondence Principles

Schapery (1984) pioneered the concept of correspondence principles. In theory of linear viscoelasticity, correspondence principles known as elastic viscoelastic relationships involving LT stresses and displacements. The LT governing equations for the viscoelastic body ($\bar{\sigma} = Es\bar{\varepsilon} = \tilde{E}\bar{\varepsilon}$) are identical to LT governing equations for the elastic body ($\bar{\sigma} = E\bar{\varepsilon}$) except $\tilde{c}_{ijke}\left(i.e.\tilde{E}\ and\ \tilde{v}\right)$ appear in viscoelastic ones instead c_{ijke}(i.e.$E\ and\ v$) of in the elastic case. Therefore, the viscoelastic solution can be determined from an elastic solution of a corresponding case by working in a LT domain with the substitution of modulus of elasticity and Poisson's ratio with Carson Transformed $E\ and\ v\ \left(i.e.\tilde{E}\ and\ \tilde{v}\right)$. The correspondence principles facilitate obtaining a viscoelastic solution from an elastic solution.

3.3.2.1 CP-I

The first correspondence principle (CP-I) is limited to time-independent surfaces. The viscoelastic solution in this case is:

$$\sigma_{ij} = \{E_1 d\sigma_{ij}^R\} = \frac{1}{E_R}\int_{-\infty}^{t} E(t-\tau)\frac{\partial \sigma_{ij}^R}{\partial \tau}\partial\tau \tag{43}$$

$$u_i = \{D du_i^R\} = E_R \int_{-\infty}^{t} D(t-\tau)\frac{\partial u_i^R}{\partial \tau}\partial\tau \tag{44}$$

where the braces { } denote a convolution integral, σ_{ij} and u_i are the stresses and displacements where $(i, j = 1, 2, 3)$, superscript R denotes the elastic media, and E_R is the reference modulus. Also, σ_{ij}^R and u_i^R are not the physical variable they known as pseudo stresses and pseudo displacements.

The viscoelastic solution satisfies the equations of the reference elastic problem with the boundary conditions,

$$\sigma_{ij}^R n_j = T_i^R \equiv \frac{-\partial \Phi_\tau}{\partial u_i^R} \qquad \text{on } S_T \tag{45}$$

$$u_i^R = U_i \equiv \{E\mathrm{d}u_i\} \qquad \text{on } S_U \tag{46}$$

where T_i^R is the surface tractions, n_j is the outer unit normal of an area element defined in the undamaged state, and Φ is the pseudo energy. The total surface is $S = S_U + S_T$.

3.3.2.2 CP-II

If S_T and S_U vary with time, certain challenges appear. For instance, if $\frac{dS_T}{dt}$ is not equal to zero on S_T, then the first correspondence principle is not valid for time-dependence. Therefore, for this type of boundary value problem, the second correspondence principle (CP-II) can be used by assuming $E_1 = E_{R1}$. When $\frac{dS_T}{dt} \geq 0$, the viscoelastic solution is:

$$\sigma_{ij} = \sigma_{ij}^R \tag{47}$$

$$u_i = \{Dd u_i^R\} = E_R \int_{-\infty}^{t} D(t-\tau) \frac{\partial u_i^R}{\partial \tau} \partial \tau \tag{48}$$

where σ_{ij}^R and u_i^R satisfies the equations of the reference elastic problem with the boundary conditions in Eqs. (45) and (46) in which $T_i^R \equiv T_i$.

3.3.2.3 CP-III

The third correspondence principle (CP-III) can be used if $\frac{dS_T}{dt} \leq 0$ and $\frac{\partial n_i}{\partial t} = 0$. The solution of viscoelastic in this case is:

$$\sigma_{ij} = \left\{E d\sigma_{ij}^R\right\} \tag{49}$$

$$u_i = u_i^R \tag{50}$$

where σ_{ij}^R and u_i^R satisfies the equations of the reference elastic problem with the traction boundary conditions in Eq. (46) and $u_i^R = U_i$ on S_U.

The second and third correspondence principles can be applied for the healing process. They are not limited to crack problems. This work is concerned with microdamage healing effect. The third correspondence principle (CP-III) will be used in predicting influence of microdamage healing on stress and displacement fields in viscoelastic media. The problem in elastic media is defined by equilibrium equations with a body forces F_i^R, strain-displacement equations, and stress-strain equations:

$$\frac{\partial \sigma_{ij}^R}{\partial x_j} + F_i^R = 0 \tag{51}$$

$$\varepsilon_{ij}^R = \frac{1}{2}\left(\frac{\partial u_i^R}{\partial x_j} + \frac{\partial u_j^R}{\partial x_i}\right) \tag{52}$$

$$\varepsilon_{ij}^{R} = \frac{1}{E_R}\left[(1+v)\sigma_{ij}^{R} - v\delta_{ij}\sigma_{kk}^{R}\right] \tag{53}$$

where δ_{ij} is the Kronecker delta (i. e. , $\delta_{ij} = 1$ if $i = j$ and $\delta_{ij} = 0$ if $i \neq j$) and $k = 1,2,3$.

Convolution integrals are used in order to obtain T_i and F_i in the viscoelastic problem since they are not the same as F_i^R and T_i^R in the elastic problem:

$$F_i^R \equiv \{D\ dF_i\} \tag{54}$$

$$T_i^R \equiv \{D\ dT_i\} \tag{55}$$

The displacements are the same for elastic and viscoelastic problems,

$$U_i^R = U_i \tag{56}$$

3.3.3 Crack Closing and Bonding in Viscoelastic Media

Schapery (1989) investigated the crack shortening in viscoelastic media. The author developed a theory to predict the process of bonding and the healing of internal cracks. Interfacial forces of attraction and external loading were studied as to how they affect the rate of growth of bonded area. The study was done for the opening mode, and other modes of fracture were not considered. Figure 12 illustrates the normal stress and displacement along the bond surface in the vicinity of the crack tip.

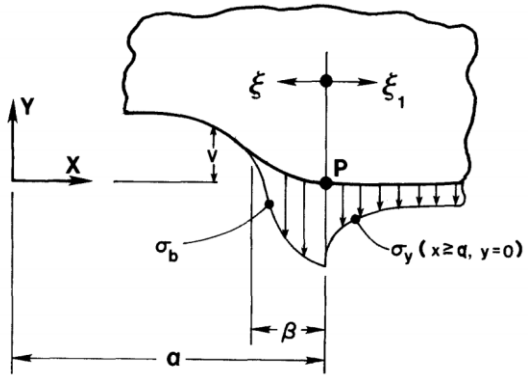

Figure 12 Normal stress and displacement along the bond surface in the vicinity of the crack tip (Schapery, 1989).

The opening displacement v above the bond surface in the vicinity of the crack tip can be obtained from CP-III:

$$v = C_R \int_0^{\beta} \sigma_b^R(\xi') F\left(\frac{\xi'}{\xi}\right) d\xi' \tag{57}$$

where

$$F\left(\frac{\xi'}{\xi}\right) \equiv \frac{2}{\pi}\left[2\left(\frac{\xi}{\xi'}\right)^{\frac{1}{2}} - ln\left|\frac{1+\left(\frac{\xi'}{\xi}\right)^{\frac{1}{2}}}{1-\left(\frac{\xi'}{\xi}\right)^{\frac{1}{2}}}\right|\right] \tag{58}$$

and

$$C_R \equiv \frac{(1-v^2)}{E_R} \tag{59}$$

The counterpart of surface normal stress σ_b^R in elastic media is obtained from the following equation:

$$\sigma_b^R = \{D\ d\sigma_b\} = E_R \int_{-\infty}^{t} D(t-\tau)\frac{\partial \sigma_b}{\partial \tau}\partial\tau \tag{60}$$

The Barenblatt is used in order to remove the stress singularity at the tip of crack. The stress intensity factor (K_I^R) in elastic media is expressed as follows:

$$K_I^R = \left(\frac{2}{\pi}\right)^{\frac{1}{2}} \int_0^{\beta} \sigma_b^R(\xi)\xi^{-\frac{1}{2}} d\xi \tag{61}$$

The surface normal stress σ_b is assumed to be independent of time and is uniform over $0 < \xi < \beta$. Also, bonding speed $\dot{a}_c$ is assumed to be independent of time during the time it takes for the crack tip to move the distance β. The work per unit surface area done on the particle by σ_b is $\sigma_b v_b$, where v_b is the opening displacement at $\xi = \beta$, assuming that $v = 0$ at $\xi = 0$. The work

for the upper surface of the crack can be added to the work for lower surface of the crack in order to obtain the bond energy $2\Gamma_b$.

Creep compliance is represented by the power law as follows:

$$D(t) = D_0 + D_1 t^m \tag{62}$$

where D_0, D_1,and m are positive constants and $0 < m \leq 1$.

The σ_b^R in elastic media can be expressed as:

$$\sigma_b^R = E_R \sigma_b \left[D_0 + D_1 (1-\eta)^m \left(\frac{\beta}{\dot{a}_b} \right)^m \right] \tag{63}$$

where $\eta \equiv \frac{\xi}{\beta}$.

Substitute Eq. (63) into Eq. (61)

$$K_I^R = \left(\frac{8}{\pi} \right)^{\frac{1}{2}} E_R \sigma_b \, \beta^{\frac{1}{2}} \left[D_0 + D_1 \gamma_m \left(\frac{\beta}{\dot{a}_b} \right)^m \right] \tag{64}$$

where

$$\gamma_m \equiv \left(\frac{\pi}{4} \right)^{\frac{1}{2}} \frac{\Gamma(1+m)}{\Gamma(1.5+m)} \tag{65}$$

where $\Gamma(\cdot)$ is the gamma function.

In order to obtain the displacement at $\xi = \beta$, Eq. (63) can be used in Eq. (57). Therefore, the work can be obtained by using the following equation:

$$W_b \equiv \sigma_b \upsilon_b = \frac{4}{\pi} (1-\nu^2) \sigma_b^2 \beta \left[D_0 + D_1 c_m \gamma_m \left(\frac{\beta}{\dot{a}_b} \right)^m \right] \tag{66}$$

where

$$c_m \equiv \frac{(2m+1)}{(m+1)} \tag{67}$$

The bonding-zone length or healing process zone β and bonding speed $\dot{a}_c$ is assumed to be a constant and obtain as follows:

$$\frac{\beta}{\beta_m} = Z(1+\lambda)^{-2}{c_m}^2 \tag{68}$$

where

$$\beta_m \equiv \frac{\pi \Gamma_b'}{2\sigma_b^2}(1-\nu^2)D_0^+{c_m}^2 \tag{69}$$

where Γ_b' is the effective bond energy, and superscripts (+) denote quantities above the bond plane. Also,

$$\frac{\dot{a}_b}{\dot{a}_m} = Z(1+\lambda)^{-2}\lambda^{-\left(\frac{1}{m}\right)}{c_m}^{\left(\frac{2+1}{m}\right)} \tag{70}$$

where

$$\dot{a}_m \equiv \beta_m \left(\frac{D_1\gamma_m}{D_0 c_m}\right)^{\frac{1}{m}} \tag{71}$$

The parameter λ is a function of Z and defined as follows:

$$\lambda = 0.5\left[c_m Z + (c_m Z)^{\frac{1}{2}}\left(c_m Z + \frac{4}{c_m} - 4\right)^{\frac{1}{2}}\right] - 1 \tag{72}$$

$$Z \equiv \left(\frac{K_I^R}{K_{I0}^R}\right) \tag{73}$$

where $(K_{I0}^R)^2 \equiv \frac{4\Gamma_b' D_0^+ (E_R^+)^2}{(1-\nu^2)}$.

4. MICRODAMAGE HEALING

This study aims to assess the influence of microdamage healing on stress intensity factor (SIF), displacement, and stress fields in proximity to the crack tip in elastic media. The model used in this work combined the effects of both instantaneous healing (short-term) and time-dependent bond strength (long-term). Also, the results of stress and displacement fields in elastic media are translated into viscoelastic media using the third correspondence principle (CP-III). Several cases are considered in this study as shown in the following flowchart.

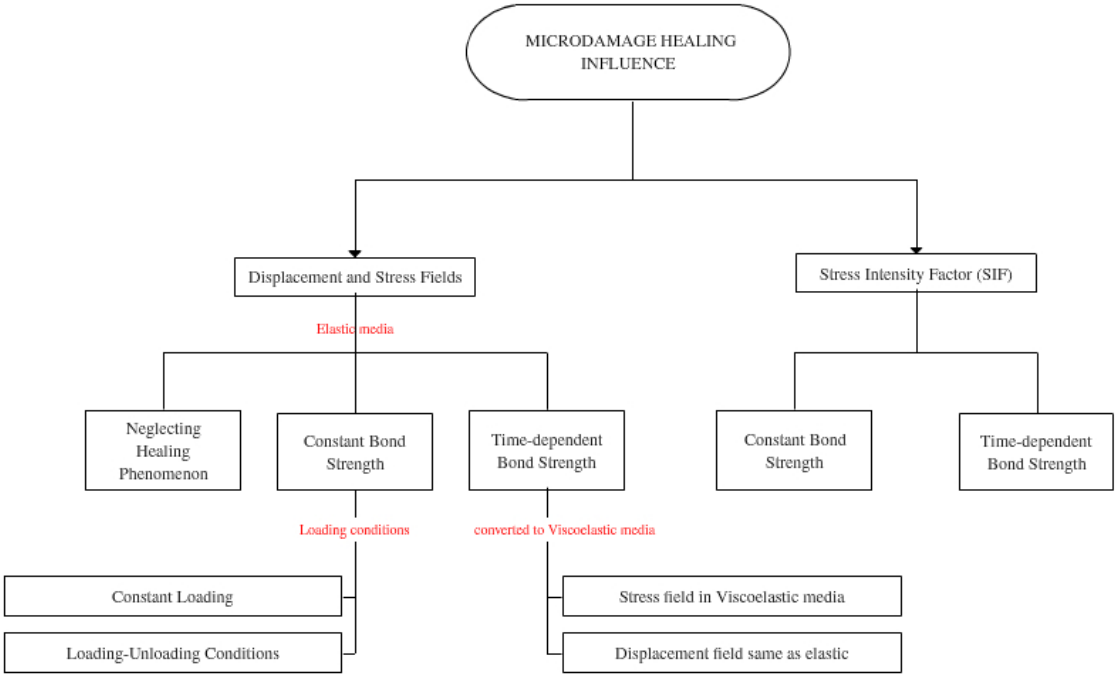

Figure 13 Cases considered in the research.

4.1 Influence of Microdamage Healing on Stress Intensity Factor

In this section the influence of microdamage healing on SIF is investigated. SIF parameter was developed to describe the state of stress at a crack tip and is used in order to establish failure criterion as a result of fracture. In order to study the effect of healing on SIF, an infinite plate with an internal crack of length *2a* subjected to far field stress σ_{∞}^{R} at infinity as shown in Figure 14 is considered. Crack surfaces are traction free in the absence of a bonding zone length β whereas crack surfaces are subjected to the bond strength σ_b when the healing mechanism is considered.

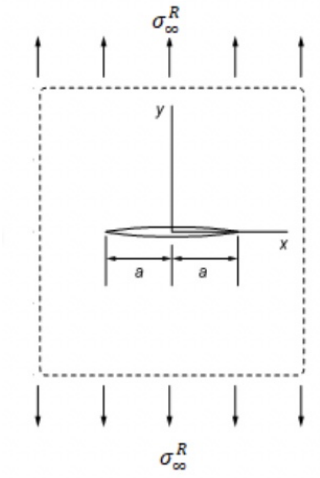

Figure 14 An infinite plate with an internal crack in subjected to far field stress.

4.1.1 Constant Bonding Strength in Elastic Media

The SIF in the existence of the microdamage healing mechanism is determined. As shown in Figure 15(a), only a quarter of the plate containing an internal crack is considered due to the symmetric boundary conditions. Also, the superposition principle is used since the material is assumed to be linearly elastic. Consequently, the case illustrated in Figure 15(a) is decomposed to the following sub-cases:

1. Far field stress applied to the plate with an internal crack as shown in Figure 15(b).

2. Induced bond strength within the healing process zone is considered in Figure 15(c).

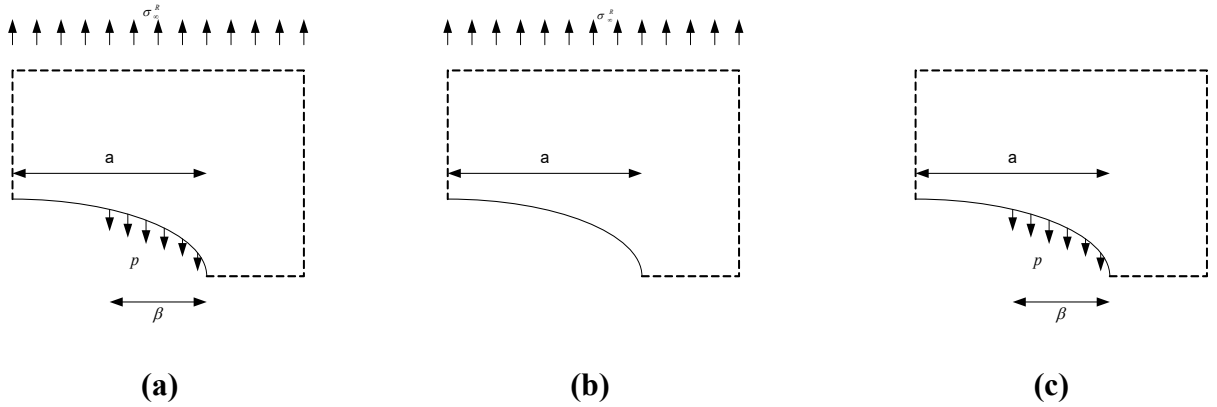

(a) **(b)** **(c)**

Figure 15 Crack of length a in a quarter of an infinite plate with far field stress σ_{∞}^{R} in the existence of the microdamage healing.

In order to compute SIF in Figure 15(c), the superposition is also applied, and it is decomposed to two sub-cases:

1. Traction field is applied in the entire crack length as illustrated in Figure 16(b).
2. Another equal and opposite force is applied in the region of $-(a-\beta)\ to\ (a-\beta)$ as illustrated in Figure 16(c).

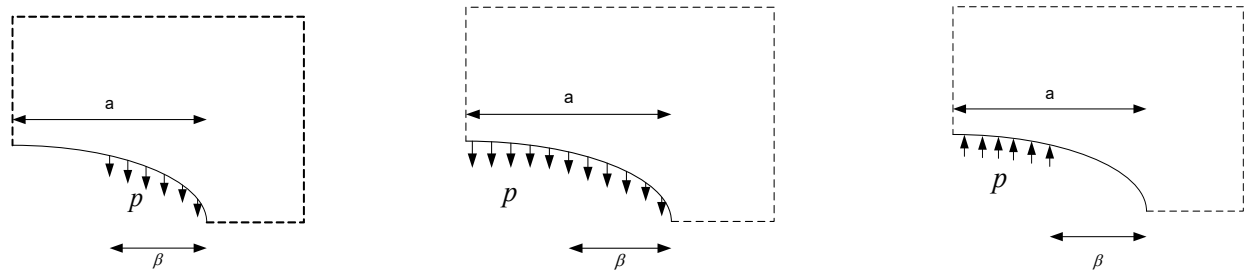

(a) **(b)** **(c)**

Figure 16 Decomposing stresses illustrated in Figure 15(c).

Using the definition of SIF, we find:

$$K_I = \sigma_\infty^R \sqrt{\pi a} \tag{74}$$

The stress function has the value of $-p$ in Figure 15(c). So, the SIF is expressed as follows:

$$K_I = -p\sqrt{\pi a} \tag{75}$$

Stress intensity factor for the crack loaded with traction can be obtained from the following equation:

$$K_I = \frac{1}{\sqrt{\pi a}} \int_{-a}^{a} \mathrm{g}_2(\xi) \sqrt{\frac{a+\xi}{a-\xi}}\, d\xi \tag{76}$$

where $\mathrm{g}_2(\xi)$ is the stress function near the crack tip (Hellan, 1985; Sedov,1972).

Substituting the value of $\mathrm{g}_2(\xi)$ in Eq. (76), the SIF will be expressed as follows:

$$K_I = \frac{p}{\sqrt{\pi a}} \int_{-(a-\beta)}^{(a-\beta)} \sqrt{\frac{a+\xi}{a-\xi}}\, d\xi = \frac{2p\sqrt{a}}{\sqrt{\pi}} \arctan\left(\frac{a-\beta}{\sqrt{\beta}\sqrt{2a-\beta}}\right) \tag{77}$$

The LEFM approach is based on elasticity; therefore, the effects multiple types of loading on the crack tip stress field can be computed by linearly adding the SIF for each type of loading. Therefore, total stress intensity factor K_I^{TOTAL} due to the far field stress, bond strength, and the healing process zone is expressed as:

$$K_I^{TOTAL} = \sigma_\infty^R \sqrt{\pi a} - p\sqrt{\pi a} + \frac{2p\sqrt{a}}{\sqrt{\pi}} \arctan\left(\frac{a-\beta}{\sqrt{\beta}\sqrt{2a-\beta}}\right) \tag{78}$$

The previous equation is written in dimensionless format in order to show how SIF varies with the healing phenomenon.

$$NSIF = \frac{K_I^{TOTAL}}{\sigma_\infty^R \sqrt{\pi a}} = 1 - \frac{p}{\sigma_\infty^R} + \frac{2}{\pi}\frac{p}{\sigma_\infty^R} \arctan\left(\frac{\frac{a}{\beta}-1}{\sqrt{2\frac{a}{\beta}-1}}\right) \tag{79}$$

Eq. (79) compares the SIF with healing properties to the SIF without considering healing properties. This ratio is denoted by the normalized stress intensity factor (NSIF). The NSIF value ranges from zero to one. If NSIF=1 indicates no microdamage healing has occurred whereas if NSIF is equal to zero that indicates the microdamage has been entirely healed.

As it can be seen in Figure 17, the NSIF decreases if the ratio of healing process zone to the length of crack (β/a) increases. In this situation, the forces between the crack surfaces attempt to close the opening and consequently the SIF value decreases. Moreover, it is obvious that the far field stress must be greater when the effect of healing is considered in order to propagate the crack and to reach a specific crack opening. On the other hand, the NSIF decreases if the ratio of constant bonding strength to the far field stress (p/σ_∞^R) increases as shown in Figure 18.

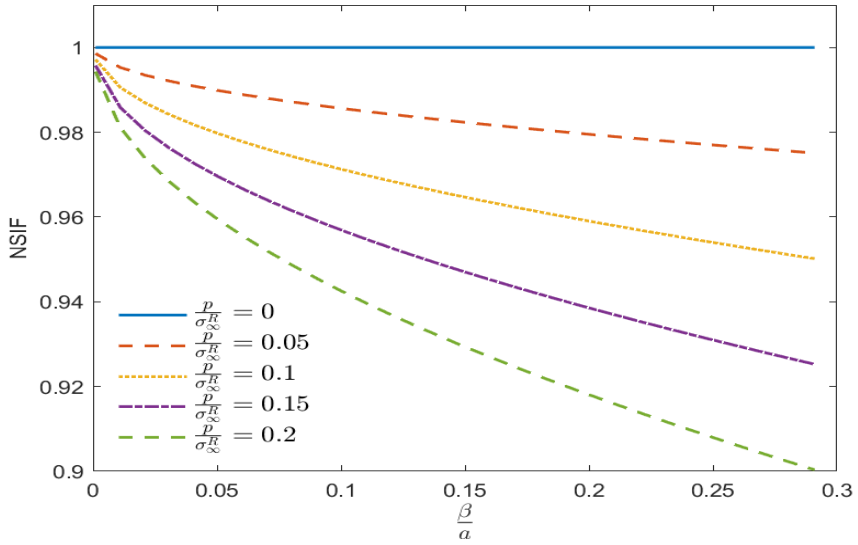

(a)

Figure 17 Influence of healing on the SIF in case of constant bonding strength. The ratio of p/σ_∞^R is constant for each set of data.

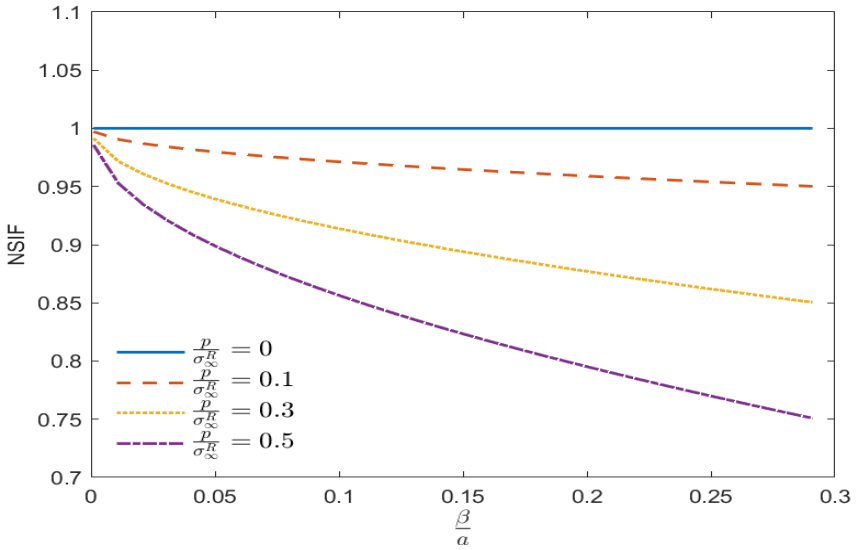

(b)

Figure 17 Continued.

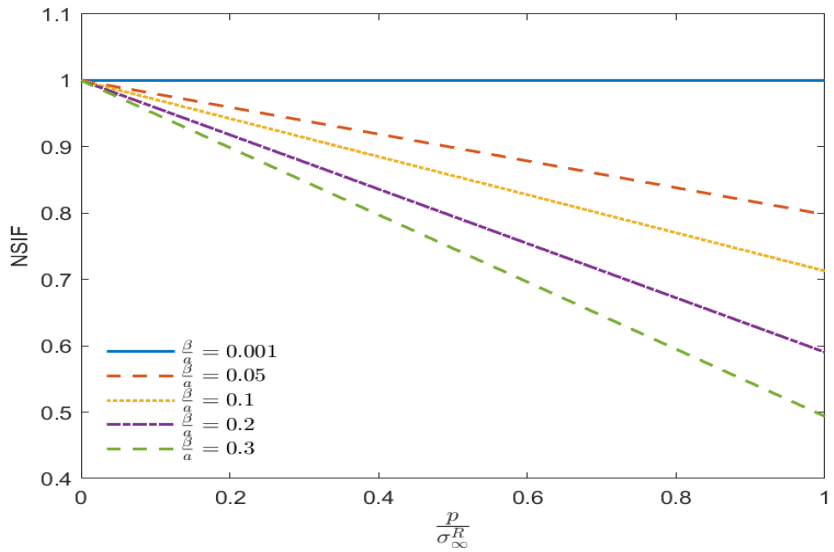

Figure 18 Influence of healing on the SIF at constant bonding strength. The ratio of β/a is constant for each set of data.

4.1.2 Time-dependent Bonding Strength in Elastic Media

During the rest periods, surface free energy caused the wetting surfaces of the micro-cracks to come into contact. Therefore, mechanical property and surface free energy are thought to be significant factors. Short-term and long-term healing result from cohesion and intermolecular diffusion. Previously, the bonding strength p is assumed to be constant. In this phase, the bonding strength is no longer constant to study the influence of both instantaneous and time-dependent bonding strength. The time-dependent bonding strength is expressed as follows:

$$\sigma_b(t) = \sigma_0 + (\sigma_b(t_\infty) - \sigma_0)\left(\frac{t}{t_\infty}\right)^{0.25} \tag{80}$$

where σ_0 is the initial bonding strength, $\sigma_b(t_\infty)$ is the bonding strength at t_∞, t is the current time, and t_∞ is the time required for the healing process to be completed.

Consequently, the bond strength as a result of healing is expressed as instantaneous and transient components as follows:

$$\sigma_b(t) = \sigma_0 + \Delta\sigma \tag{81}$$

where σ_0 is the instantaneous bonding strength and $\Delta\sigma$ is the transient part of the bonding strength. The bonding strength will not affect the integral in Eq. (76) because it is assumed to be independent of the spatial factor. Therefore, the Eq. (79) is also valid for time-dependent bonding strength case. Substituting into Eq. (79) and replacing p by $\sigma_b(t)$ yields

$$\text{NSIF} = 1 - \frac{\sigma_0 + (\sigma_b(t_\infty) - \sigma_0)\left(\frac{t}{t_\infty}\right)^{0.25}}{\sigma_\infty^R} + \frac{2}{\pi}\frac{\sigma_0 + (\sigma_b(t_\infty) - \sigma_0)\left(\frac{t}{t_\infty}\right)^{0.25}}{\sigma_\infty^R} arctan\left(\frac{\frac{a}{\beta} - 1}{\sqrt{2\frac{a}{\beta} - 1}}\right) \tag{82}$$

As it can be seen in Figure 19, as the healing process increases over time, the bonding strength increases, and therefore the NSIF decreases for the constant ratio of healing process zone

to the length of crack (β/a). Moreover, the NSIF decreases due to the increase of the ratio of (β/a) for a fixed value of time.

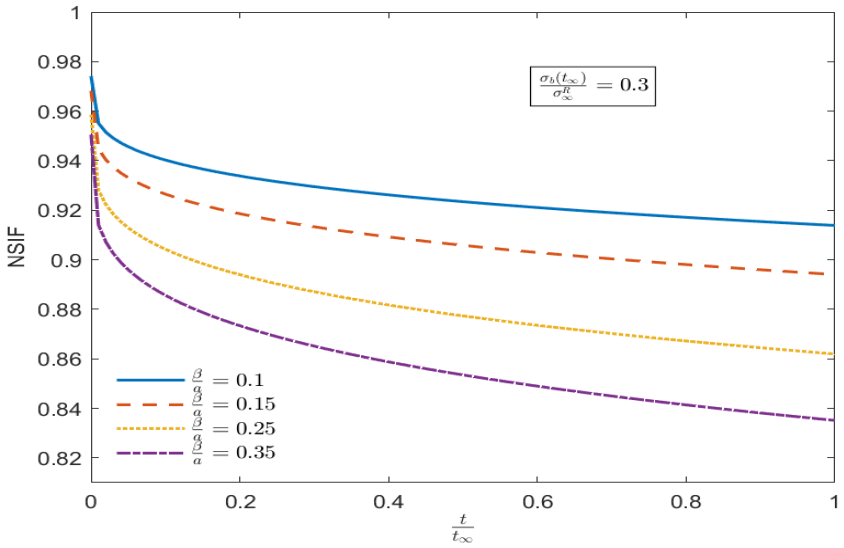

(a)

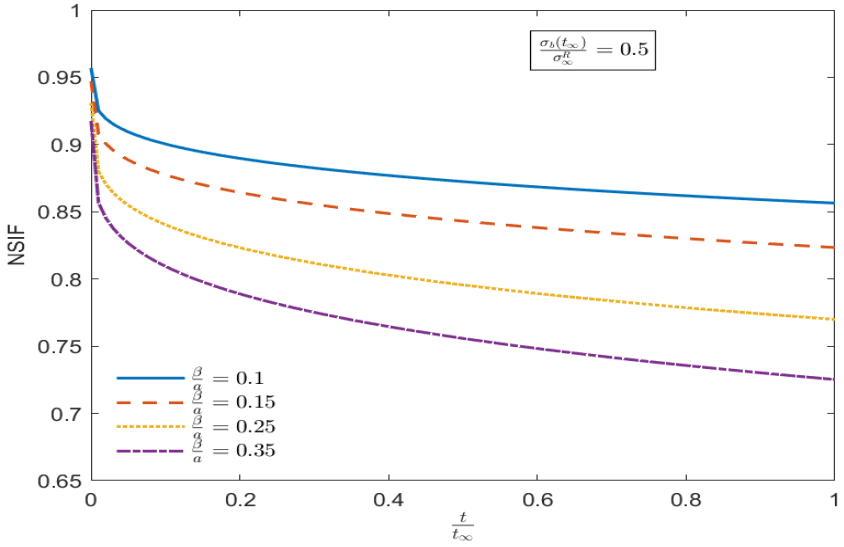

(b)

Figure 19 Influence of time on the NSIF. The ratio of β/a is constant for each set of data.

4.2 Influence of Microdamage Healing on Displacement and Stress fields

In this section the influence of microdamage healing on displacement and stress fields in elastic media are investigated in the following different cases.

4.2.1 Neglecting the Influence of Healing Process

The stress and displacement fields are calculated using the complex variable method. A superposition principle is taken as sketched in Figure 15(b).

For the crack surface loading part of the problem:

$$\phi'_{\mathrm{I}} = \frac{\sigma_{\infty}^{R}}{\pi\sqrt{\mathrm{z}^2 - \mathrm{a}^2}} \int_{-\mathrm{a}}^{\mathrm{a}} \frac{\sqrt{\mathrm{a}^2 - \xi^2}}{\mathrm{z} - \xi}\, \mathrm{d}\xi \tag{83}$$

Evaluating this integral yield:

$$\phi'_{\mathrm{I}} = \frac{\sigma_{\infty}^{R}\, z}{\sqrt{\mathrm{z}^2 - \mathrm{a}^2}} - \sigma_{\infty}^{R} \tag{84}$$

which can be integrated to yield:

$$\phi_I = \sigma_{\infty}^{R}\sqrt{\mathrm{z}^2 - \mathrm{a}^2} - \sigma_{\infty}^{R} z + constant \tag{85}$$

Superposing the far field stress with the stress given by the stress functions, Eq. (29), yields $\sigma_{22} = Re\, \emptyset' + \sigma_{\infty}^{R}$. Substituting in ϕ'_{I} from Eq. (84) yields:

$$\sigma_{22} = Re\left(\frac{\sigma_{\infty}^{R}\, z}{\sqrt{\mathrm{z}^2 - \mathrm{a}^2}} - \sigma_{\infty}^{R}\right) + \sigma_{\infty}^{R} \tag{86}$$

Evaluating the stresses along $z = x$

$$\sigma_{22} = Re\left(\frac{\sigma_{\infty}^{R}\, x}{\sqrt{\mathrm{x}^2 - \mathrm{a}^2}}\right) \tag{87}$$

Therefore,

$$\sigma_{22} = \begin{cases} 0 \quad , & |x| < a \\ \dfrac{\sigma_{\infty}^{R}\, x}{\sqrt{\mathrm{x}^2 - \mathrm{a}^2}} \, , & |x| \geq a \end{cases}$$

The displacement along the crack line can be found using Eq. (32) with ϕ_I as calculated above. The result is:

$$u_2 = \frac{1}{2G}\frac{k+1}{2} Im\left(\sigma_\infty^R \sqrt{\mathrm{z}^2 - \mathrm{a}^2} - \sigma_\infty^R z + constant\right) \tag{88}$$

Evaluating the displacements along $z = x$

$$u_2 = \pm\sigma_\infty^R \frac{k+1}{4G}\sqrt{\mathrm{a}^2 - \mathrm{x}^2} \tag{89}$$

4.2.2 Constant Bonding Strength Case in Elastic Media

The stress function derivative is defined for both cases described in Figure 15(c) and Figure 16(a). The calculation of Figure 15(c) is similar to the case in Figure 15(b) but with the difference in the value of the stress. The bond strength $(-p)$ is used instead of taking far field stress. Therefore, the stress function derivative for the case shown in Figure 15(c) is denoted by $\phi'_{\mathrm{I}}(1)$ and is expressed as follows:

$$\phi'_{\mathrm{I}}(1) = \frac{-p}{\pi\sqrt{\mathrm{z}^2 - \mathrm{a}^2}} \int_{-1}^{1} \frac{\sqrt{\mathrm{a}^2 - \mathrm{t}^2}}{\mathrm{z} - \mathrm{t}}\, \mathrm{dt} \tag{90}$$

Evaluating this integral yield:

$$\phi'_{\mathrm{I}}(1) = \frac{-p\, z}{\sqrt{\mathrm{z}^2 - \mathrm{a}^2}} + \mathrm{p} \tag{91}$$

which can be integrated to yield:

$$\phi_I(1) = p\sqrt{\mathrm{z}^2 - \mathrm{a}^2} + pz + constant \tag{92}$$

Evaluating the stresses along $z = x$

$$\sigma_{22} = Re\left(\frac{-p\, x}{\sqrt{\mathrm{x}^2 - \mathrm{a}^2}}\right) \tag{93}$$

Evaluating the displacements along $z = x$

$$u_2 = -p\frac{k+1}{4G}\sqrt{\mathrm{a}^2 - \mathrm{x}^2} \tag{94}$$

As illustrated in Figure 16(b) the bonding strength is assumed over a part of the crack surface. Therefore, the stress function derivative is denoted by $\phi'_{\mathrm{I}}(2)$ and obtained as follows:

$$\phi'_{\mathrm{I}}(2) = \frac{p}{\pi\sqrt{\mathrm{z}^2 - \mathrm{a}^2}}\int_{-(a-\beta)}^{(a-\beta)} \frac{\sqrt{\mathrm{a}^2 - \mathrm{t}^2}}{\mathrm{z} - \mathrm{t}}\,\mathrm{dt} \tag{95}$$

Evaluating this integral yield:

$$\phi'_{\mathrm{I}}(2) = \frac{2\mathrm{pz}}{\pi\sqrt{\mathrm{z}^2 - \mathrm{a}^2}} arcsin\left(\frac{a-\beta}{a}\right) - \frac{2p}{\pi} arctan\left(\frac{(a-\beta)\sqrt{\mathrm{z}^2 - \mathrm{a}^2}}{z\sqrt{2\mathrm{a}\beta - \beta^2}}\right) \tag{96}$$

$\phi'_{\mathrm{I}}(2)$ can be integrated to yield:

$$\phi_I(2) = \frac{2\mathrm{p}}{\pi} arcsin(c)\sqrt{\mathrm{z}^2 - \mathrm{a}^2} - \frac{2p}{\pi}\left(z \times arctan\left(\frac{c}{\sqrt{1-\mathrm{c}^2}}\frac{\sqrt{\mathrm{z}^2-\mathrm{a}^2}}{z}\right) - ac \times arctan\left(\frac{c}{\sqrt{1-\mathrm{c}^2}}\frac{\sqrt{\mathrm{z}^2-\mathrm{a}^2}}{z}\right)\right) \tag{97}$$

where c equal $\frac{a-\beta}{a}$.

Evaluating the stresses along $z = x$

$$\sigma_{22} = \mathrm{Re}\frac{2\mathrm{px}}{\pi\sqrt{\mathrm{x}^2 - \mathrm{a}^2}} arcsin(c) - \frac{2p}{\pi} arctan\left(\frac{c\sqrt{\mathrm{x}^2 - \mathrm{a}^2}}{x\sqrt{1 - \mathrm{c}^2}}\right) \tag{98}$$

Evaluating the displacements along $z = x$

$$u_2 = \frac{k+1}{4G}\frac{2p}{\pi} arcsin(c)\sqrt{a^2 - x^2} \tag{99}$$

Using superposition principle, the stress field is described in the following equation:

$$\sigma_{22} = Re\left(\frac{\sigma_\infty^R\, x}{\sqrt{x^2-a^2}}\right) + Re\left(\frac{-px}{\sqrt{x^2-a^2}}\right) + Re\left(\frac{2px}{\pi\sqrt{x^2-a^2}}\, arcsin\left(\frac{a-\beta}{a}\right) - \frac{2p}{\pi}\, arctan\left(\frac{(a-\beta)\sqrt{x^2-a^2}}{x\sqrt{2a\beta-\beta^2}}\right)\right) \tag{100}$$

The stress field equation is written in dimensionless format as follows:

$$\frac{\sigma_{22}}{\sigma_\infty^R} = Re\left(\frac{1}{\sqrt{1-\left(\frac{a}{x}\right)^2}}\right) + Re\left(\frac{\frac{-p}{\sigma_\infty^R}}{\sqrt{1-\left(\frac{a}{x}\right)^2}}\right) + Re\left(\frac{2}{\pi\sqrt{1-\left(\frac{a}{x}\right)^2}}\frac{p}{\sigma_\infty^R}\, arcsin\left(1-\frac{\beta}{a}\right) - \frac{2}{\pi}\frac{p}{\sigma_\infty^R}\, arctan\left(\frac{\left(1-\frac{\beta}{a}\right)\sqrt{1-\left(\frac{a}{x}\right)^2}}{\sqrt{2\frac{\beta}{a}-\left(\frac{\beta}{a}\right)^2}}\right)\right) \tag{101}$$

The left-hand side of Eq. (101) is called the normalized stress (NS). The following figures display the stress field proximal to the crack tip. The stress at the crack tip reaches infinity as mentioned earlier but farther away from the tip the stress decreases. As it can be seen in Figure 20) and (21), the NS reaches the value of $(1 - p/\sigma_\infty^R)$ if the value of (a/x) goes to infinity. In Figure 20, the value of p/σ_∞^R is assumed to be constant, whereas the ratio of bonding strength to the crack length β/a varies. For a constant value of p/σ_∞^R, the NS decreases as the value of (a/x) decreases. Additionally, the NS decreases when the bonding strength (p/σ_∞^R) increases as seen in Figure 20.

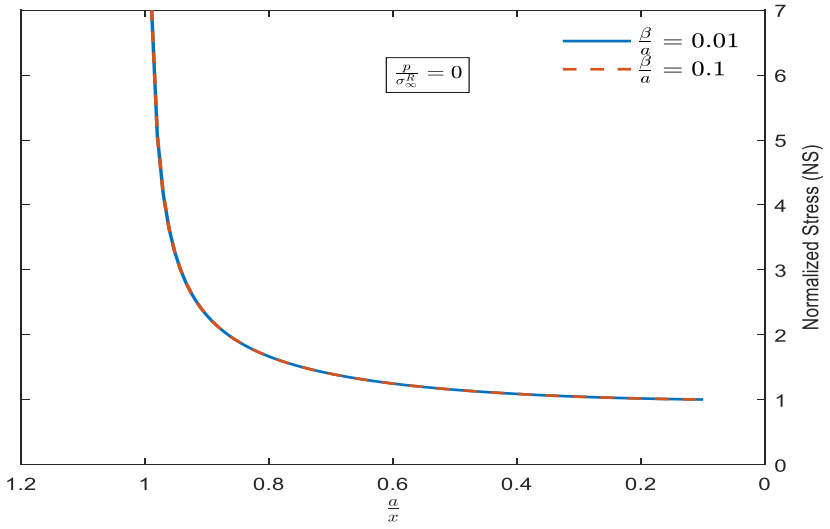

(a)

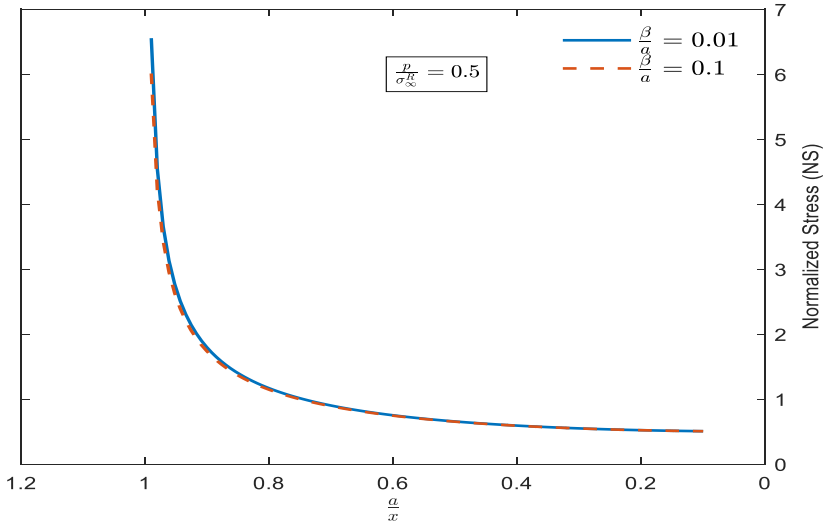

(b)

Figure 20 Influence of healing on the NS at constant bonding strength. The ratio of p/σ_∞^R is constant.

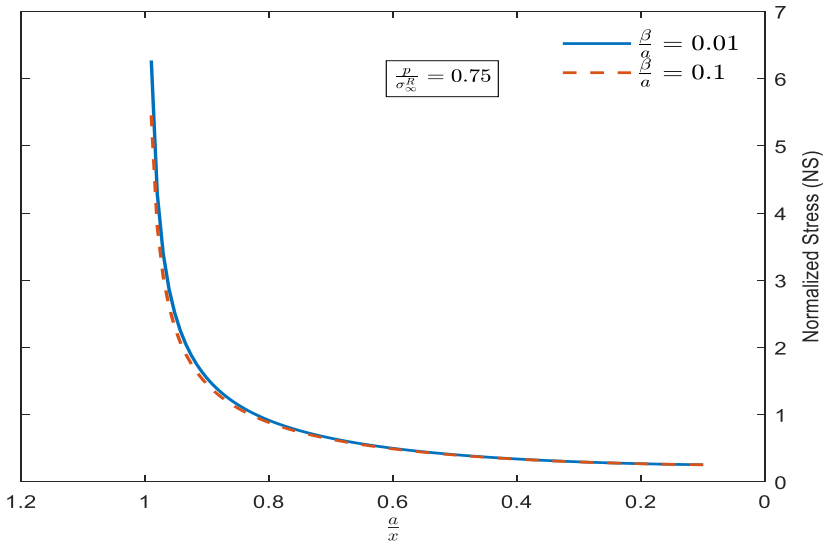

(c)

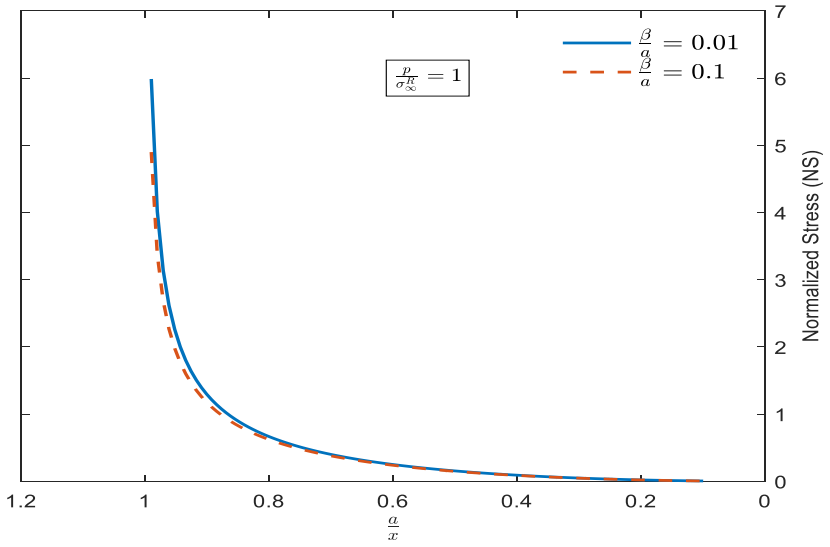

(d)

Figure 20 Continued.

Figure 21 demonstrates the effect of microdamage healing on a stress field in the vicinity of crack tip in case of constant bonding strength. In the following figure, the value of p/σ_{∞}^{R} varies whereas the value of (β/a) is constant. For a constant ratio of (β/a), the NS decreases as the value of p/σ_{∞}^{R} increases. Moreover, the NS increases when the bonding process zone increases, as it can be seen in Figure 21. If the value of p/σ_{∞}^{R} is greater than one, the stress could become compressive because it represents the case when the crack surfaces are under compressive stress states.

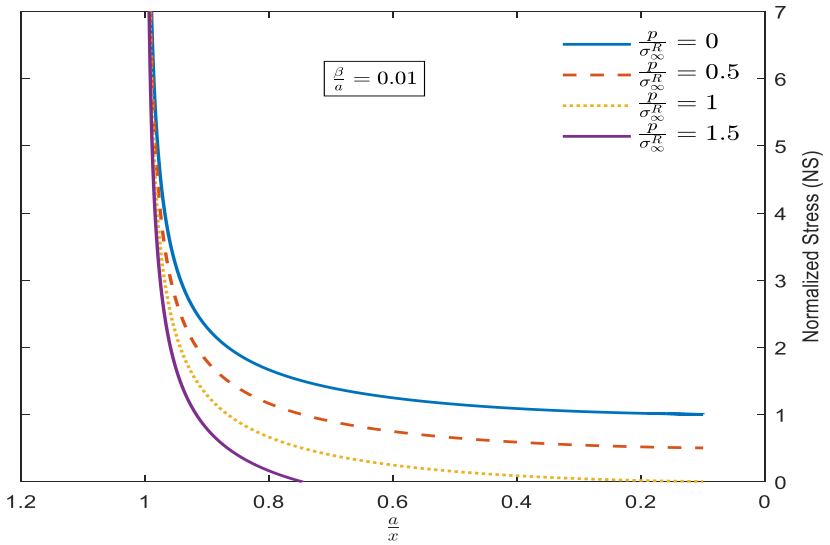

(a)

Figure 21 Influence of healing on the NS at constant bonding strength. The ratio of β/a is constant.

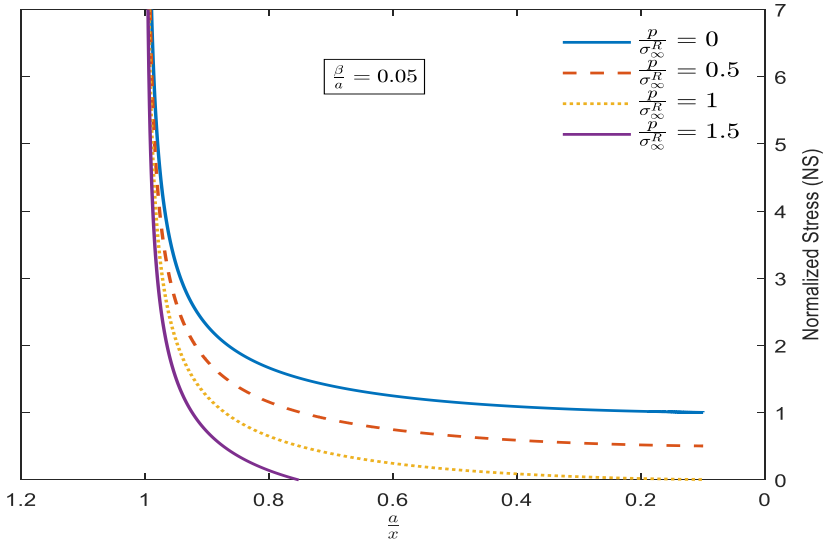

(b)

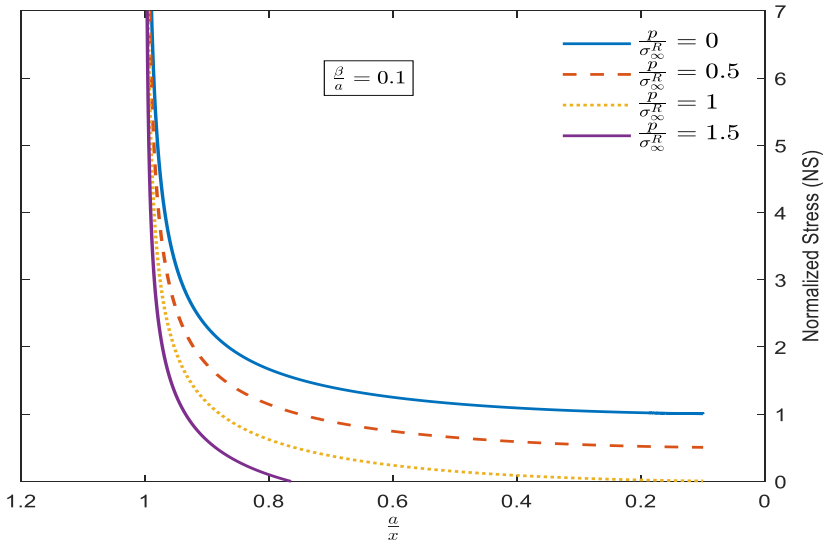

(c)

Figure 21 Continued.

The displacement field is described in the following equation:

$$u_2 = \frac{k+1}{4G}\sigma_\infty^R\sqrt{a^2-x^2} - \frac{k+1}{4G}p\sqrt{a^2-x^2} + \frac{k+1}{4G}\frac{2p}{\pi}\left(arcsin(c)\sqrt{a^2-x^2} - x \times \right.$$
$$\left. arctan\left(\frac{c}{\sqrt{1-c^2}}\frac{\sqrt{a^2-x^2}}{x}\right) + ac \times arctan\left(\frac{1}{\sqrt{1-c^2}}\frac{\sqrt{a^2-x^2}}{a}\right)\right) \quad (102)$$

The above equation is written in dimensionless format as follows:

$$\frac{u_2}{\frac{k+1}{4G}a\sigma_\infty^R} = \sqrt{1-\left(\frac{x}{a}\right)^2} - \frac{p}{\sigma_\infty^R}\sqrt{1-\left(\frac{x}{a}\right)^2} + \frac{2}{\pi}\frac{p}{\sigma_\infty^R}\left(arcsin(c)\sqrt{1-\left(\frac{x}{a}\right)^2} - \frac{x}{a} \times \right.$$
$$\left. arctan\left(\frac{c}{\sqrt{1-c^2}}\frac{\sqrt{1-\left(\frac{x}{a}\right)^2}}{\frac{x}{a}}\right) + c \times arctan\left(\frac{c}{\sqrt{1-c^2}}\sqrt{1-\left(\frac{x}{a}\right)^2}\right)\right) \quad (103)$$

The left-hand side of Eq. (103) is called the normalized displacement (NU). The following figures display the effect of microdamage healing on displacement field in the vicinity of crack tip in case of constant bonding strength. The displacement at the crack tip is equal to zero, but farther away from the tip the displacement increases. As depicted in Figure 22, the value of *c* is assumed to be constant whereas the ratio of bonding strength to the far field stress (p/σ_∞^R) varies. The NU decreases as the value of (p/σ_∞^R) increases for a constant value of *c*. This indicates that the healing process tends to decrease the distance between the crack surfaces. Also, the NU in Figure 22(b) is less than NU in Figure 22(c) as a result of a greater healing process zone.

In Figure 23, the value of *c* varies while the ratio of (p/σ_∞^R) remains constant. In other words, it shows the influence of a different bonding-zone length in displacement fields. For a constant value of (p/σ_∞^R), the NU decreases as the value of c decreases. This indicates that the distance between the upper and lower surfaces of the micro-crack decrease as a result of the healing

process. Furthermore, the NU in Figure 23(c) is less than NU in Figure 23(b) a result of a greater bonding strength.

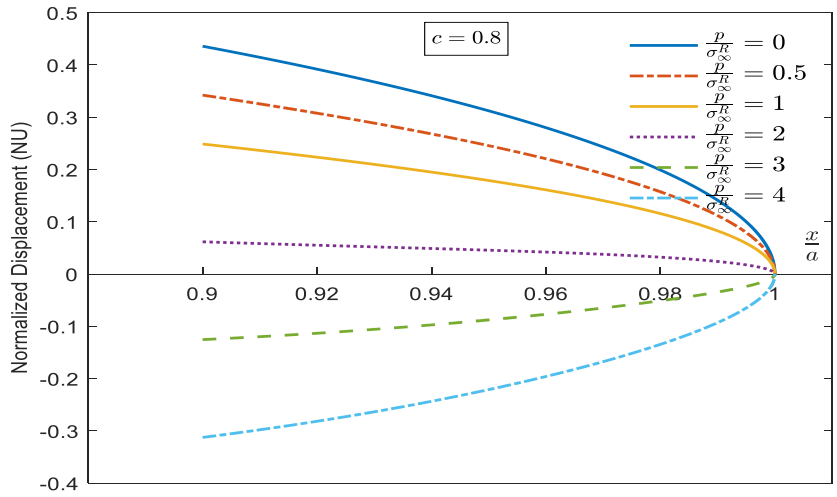

(a)

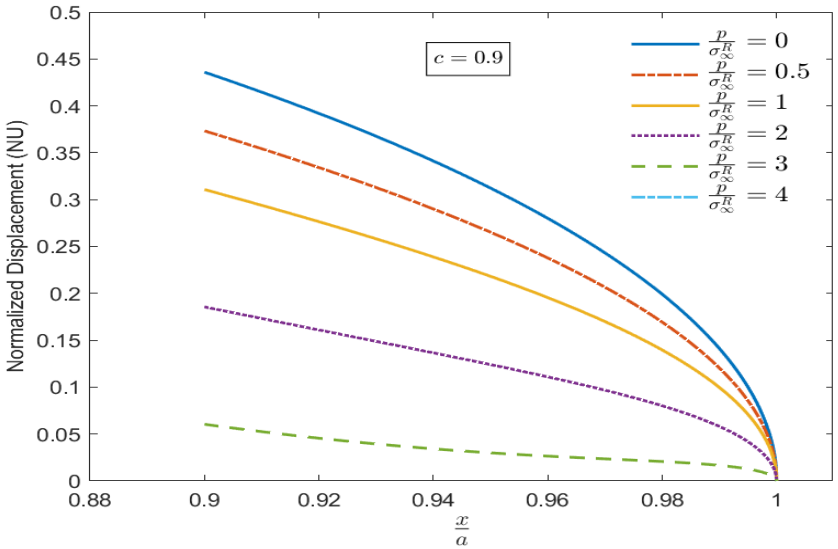

(b)

Figure 22 Influence of healing on the NU at constant bonding strength and constant value of *c*.

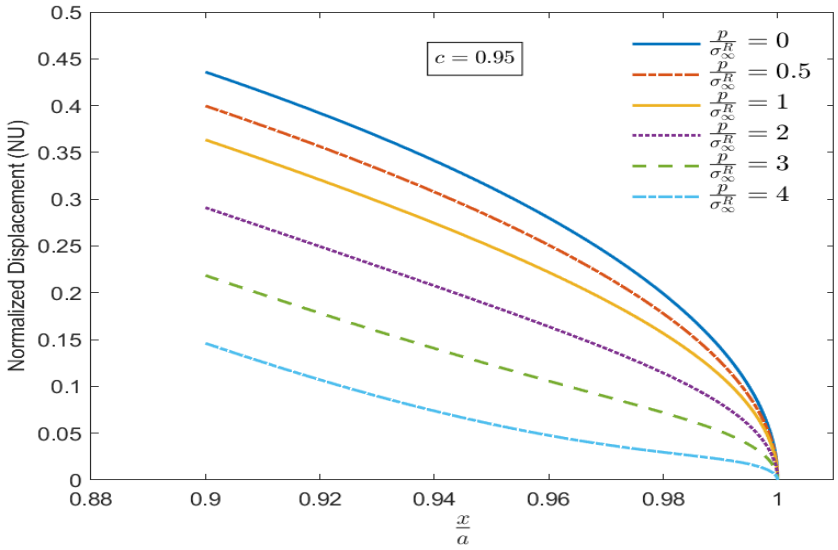

(c)

Figure 22 Continued.

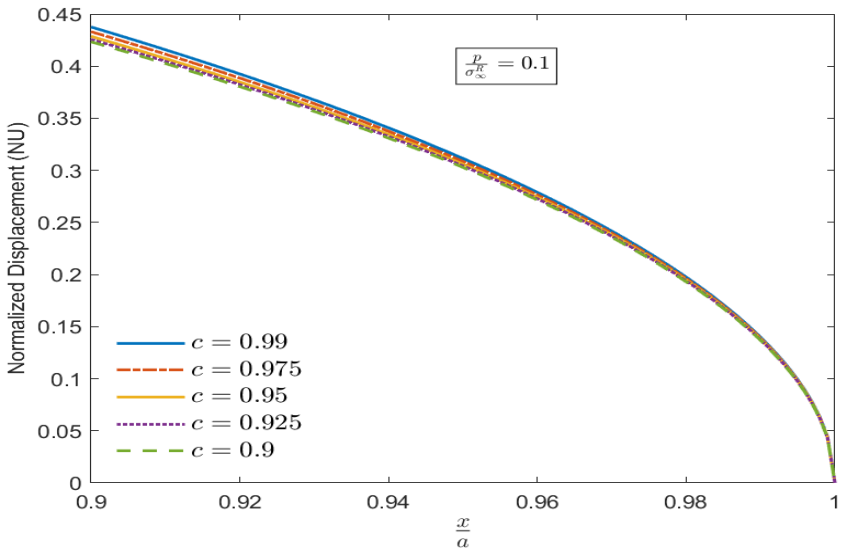

(a)

Figure 23 Influence of healing on the NU at constant bonding strength under constant value of p/σ_∞^R.

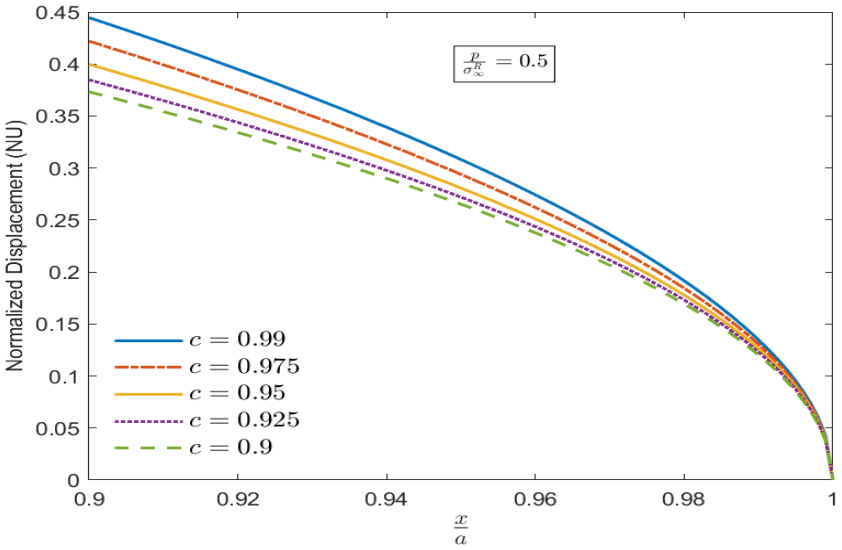

(b)

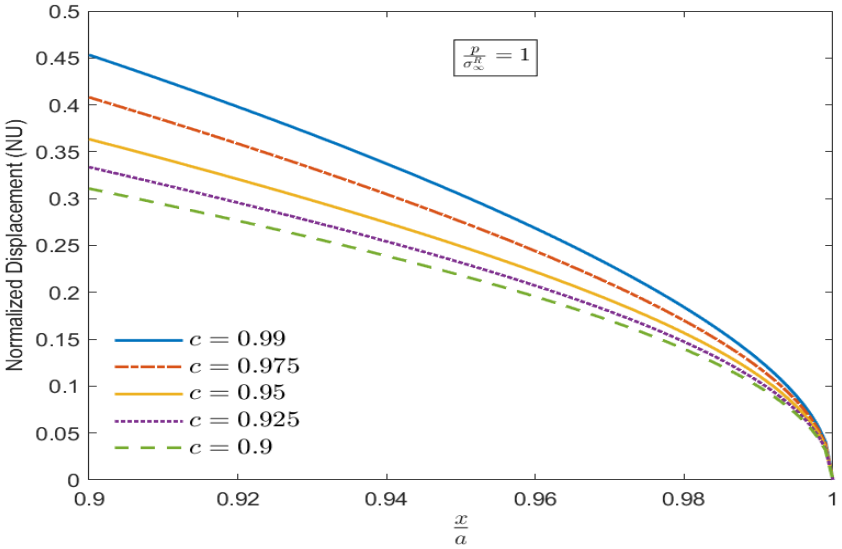

(c)

Figure 23 Continued.

4.2.3 Loading-Unloading Condition

In this section, the far field stress is no longer constant in order to demonstrate the effect of loading and unloading scenarios on stress and displacement fields. The impact of triangular loading and unloading on stress and displacement fields are studied. The period of loading and unloading cycles are considered to be equal to T. The far field stress is written in terms of σ_{∞}^{R} as follows:

$$F = \frac{\sigma_{\infty}^{R}(t)}{\sigma_{\infty}^{R}} \tag{104}$$

where F is the stress factor, F varies from zero to one as illustrated in Figure 24.

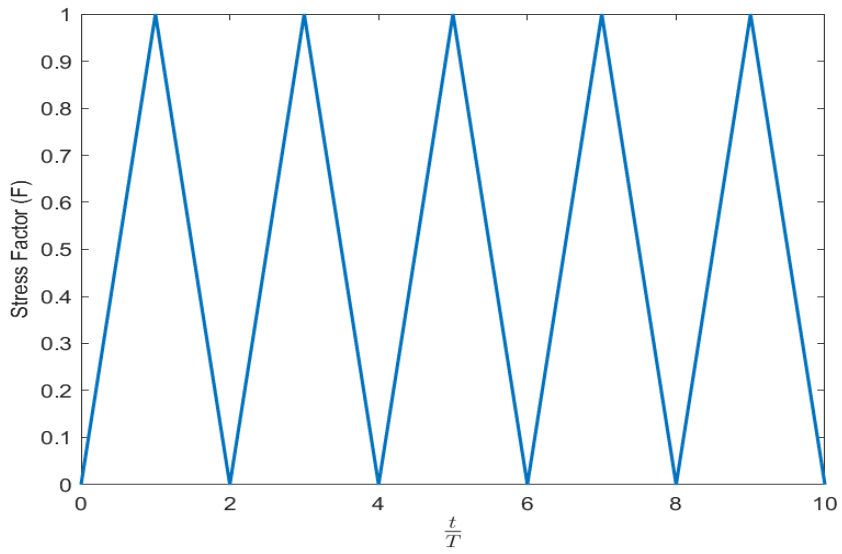

Figure 24 Far field stress loading and unloading cycles.

Stress field in case of loading and unloading condition is expressed as:

$$\frac{\sigma_{22}}{\sigma_{\infty}^{R}} = F\ \frac{1}{\sqrt{1-\left(\frac{a}{x}\right)^2}} - \frac{p}{\sigma_{\infty}^{R}}\frac{1}{\sqrt{1-\left(\frac{a}{x}\right)^2}} + \frac{2}{\pi}\frac{p}{\sigma_{\infty}^{R}}\frac{1}{\sqrt{1-\left(\frac{a}{x}\right)^2}}arcsin(c) - \frac{2}{\pi}\frac{p}{\sigma_{\infty}^{R}}arctan\frac{c\sqrt{1-\left(\frac{a}{x}\right)^2}}{\sqrt{1-c^2}} \tag{105}$$

Also, displacement field in case of loading and unloading condition as follows:

$$\frac{u_2}{\frac{k+1}{4G}a\sigma_\infty^R} = F\sqrt{1-\left(\frac{x}{a}\right)^2} - \frac{p}{\sigma_\infty^R}\sqrt{1-\left(\frac{x}{a}\right)^2} + \frac{2}{\pi}\frac{p}{\sigma_\infty^R}\left(arcsin(c)\sqrt{1-\left(\frac{x}{a}\right)^2} - \frac{x}{a}\times \right.$$

$$\left. arctan\left(\frac{c}{\sqrt{1-c^2}}\frac{\sqrt{1-\left(\frac{x}{a}\right)^2}}{\frac{x}{a}}\right) + c \times arctan\left(\frac{c}{\sqrt{1-c^2}}\sqrt{1-\left(\frac{x}{a}\right)^2}\right)\right) \tag{106}$$

The loading condition is considered if the stress factor increases. Therefore, the NU increases as shown in Figure 25. Also, the NU decreases as the ratio of (p/σ_∞^R) increases for a constant value of c as it can be seen in the Figure 25.

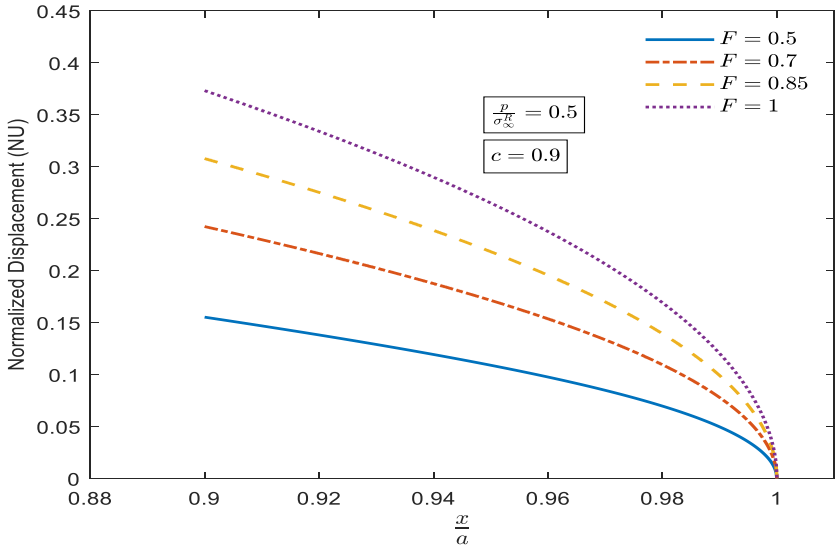

(a)

Figure 25 Influence of healing on the NU under constant value of c in loading-unloading scenarios.

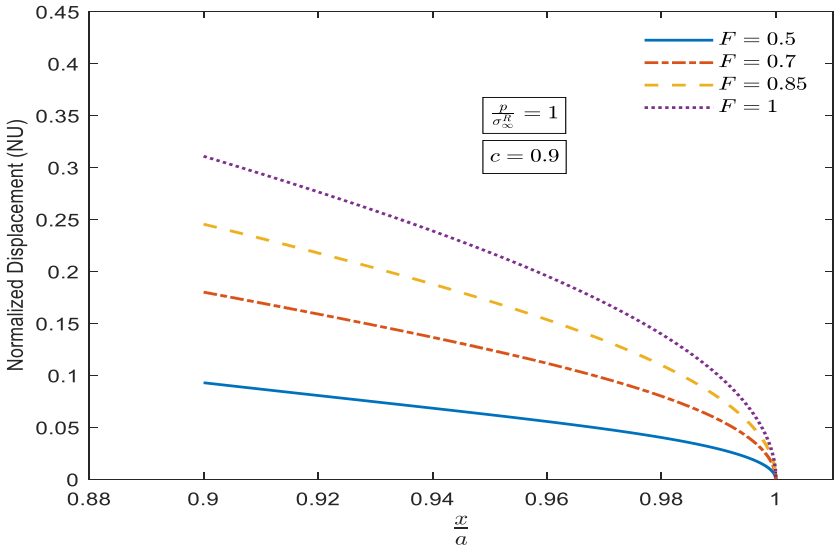

(b)

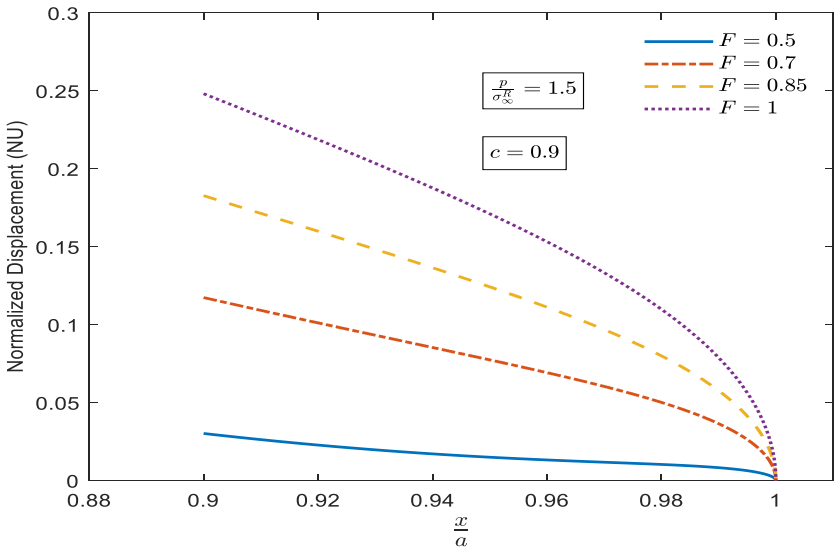

(c)

Figure 25 Continued.

Figure 26 demonstrates the displacement field in the proximity of a crack tip in a loading-unloading condition. The value of *c* is different in Figure 26 while the ratio of bonding strength to

the far field stress (p/σ_{∞}^{R}) remains constant. In other words, it shows the influence of a different healing process zone in displacement fields. For a constant value of (p/σ_{∞}^{R}), the NU increases as the value of c increases. This indicates that the healing phenomenon tends to reduce the distance between the crack surfaces. Furthermore, the normalized displacement in Figure 26(a) is less than the normalized displacement in Figure 26(b) for the region $0.90 < x < 1$ as a result of a greater bonding zone.

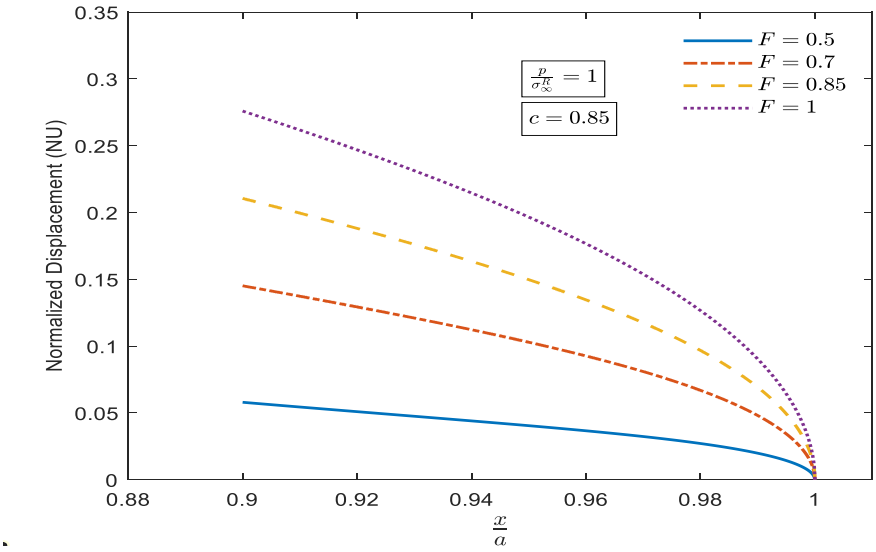

(a)

Figure 26 Influence of healing on the NU under constant value of p/σ_{∞}^{R} in loading-unloading scenarios.

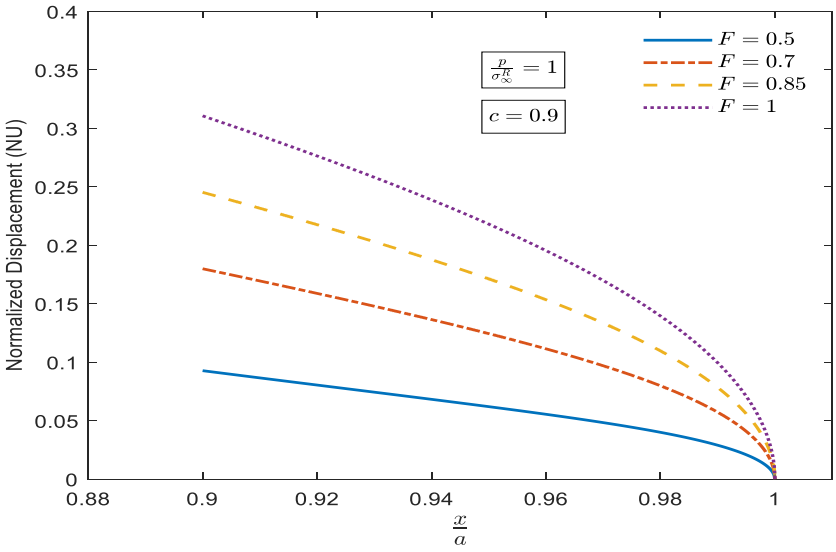

(b)

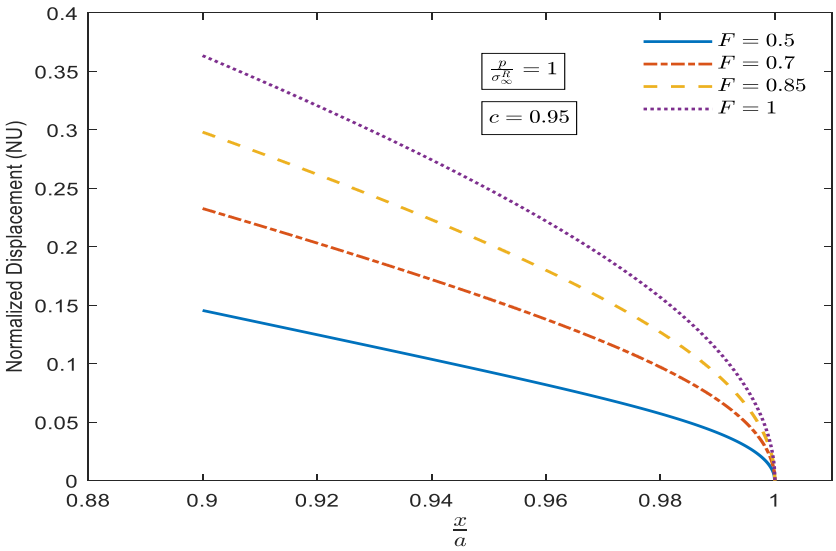

(c)

Figure 26 Continued.

The following figures show the effect of different values of stress factor c and p/σ_∞^R on the stress field. In Figure 27, the value of c is assumed to be constant and different values of p/σ_∞^R are considered. As depicted in Figure 27, an increase in the value of p/σ_∞^R results in a reduction in the

stress field consistent with the fact that the healing process tends to close the crack opening. Consequently, an increase in the stress factor produces an increase in the stress field value.

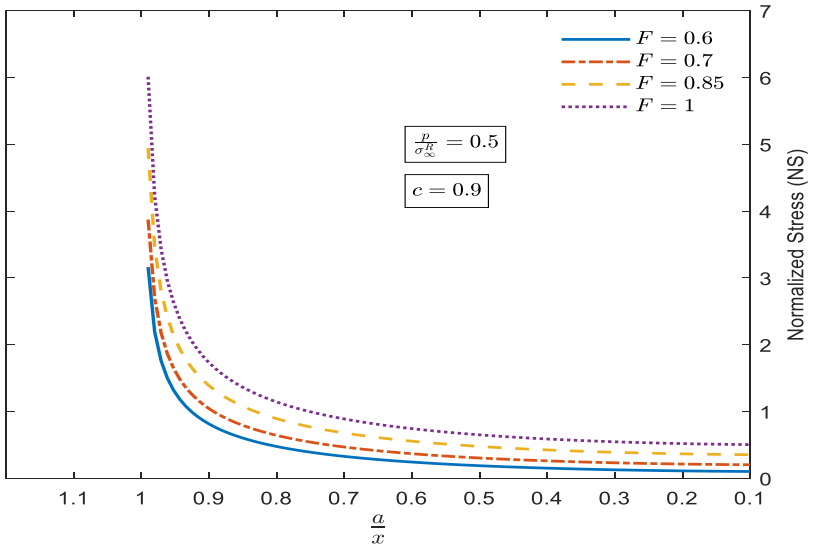

(a)

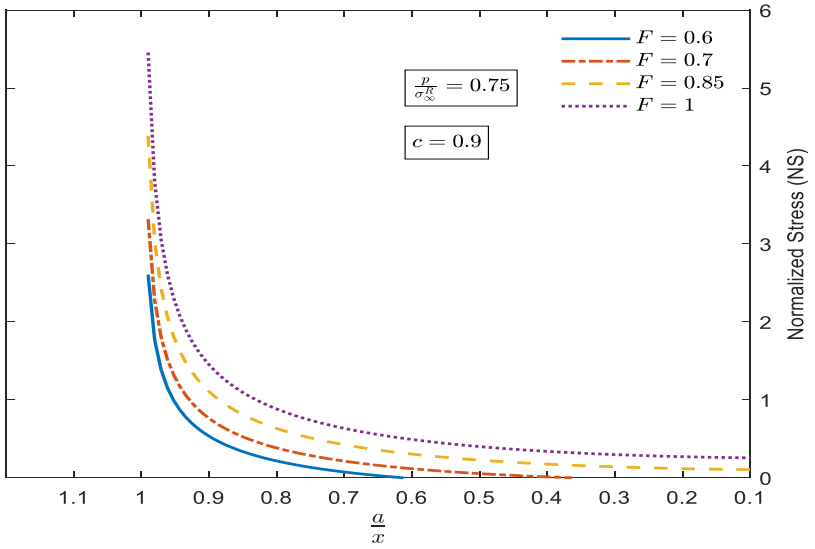

(b)

Figure 27 Effect of loading-unloading condition on stress field under constant value of c and variable value of p/σ_∞^R.

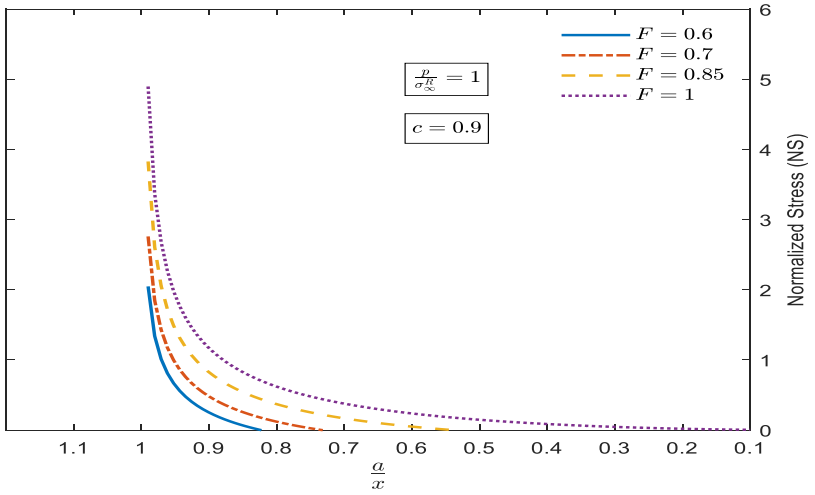

(c)

Figure 27 Continued.

In Figure 28, the value of p/σ_∞^R is assumed to be constant and different values of c are considered. As depicted in Figure 28, an escalation in the value of c causes an increase in the stress field which means that a larger healing process zone leads to more reduction on the stress field.

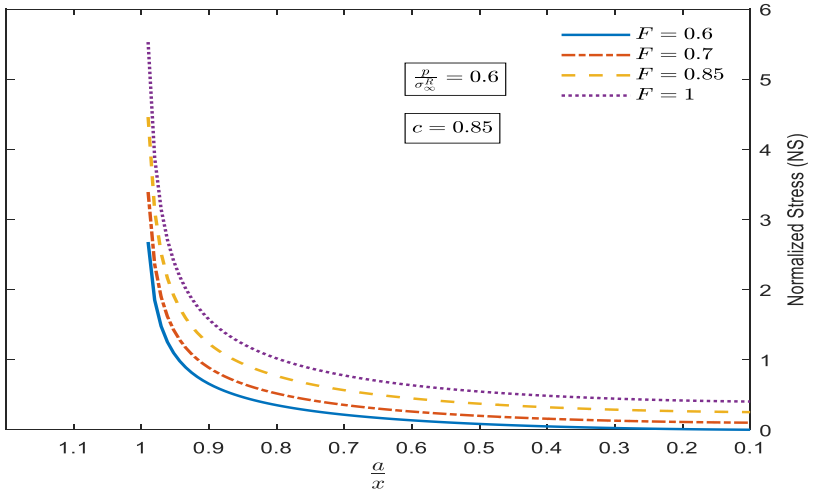

(a)

Figure 28 Effect of loading-unloading condition on stress field under constant value of p/σ_∞^R and variable value of c.

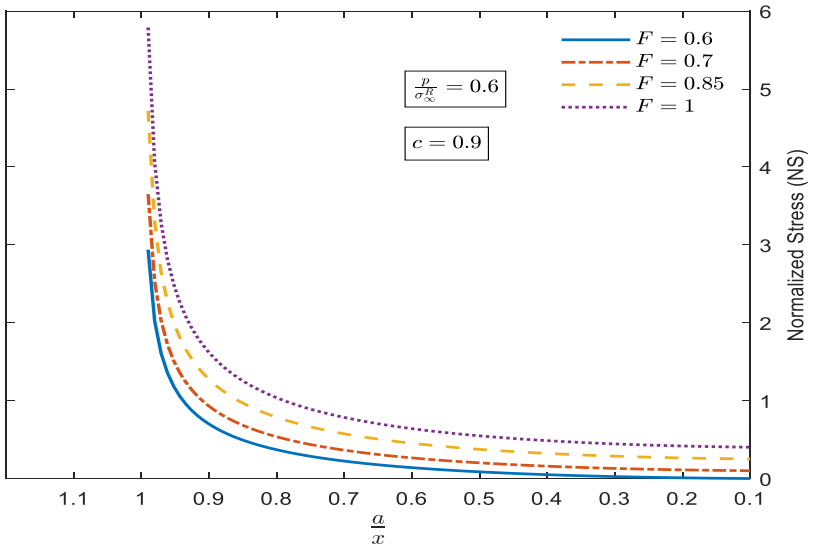

(b)

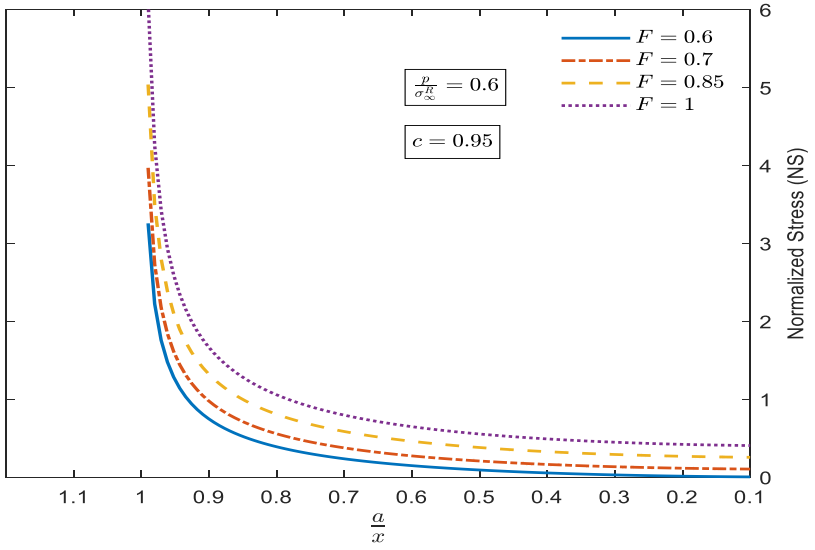

(c)

Figure 28 Continued.

4.2.4 Time-dependent Bond Strength in Elastic Media

In this case the bonding strength is dependent on time and is independent of space, so the derivative of stress function, Eq. (33), is not affected; consequently, Eqs. (100) and (102) can be used for a time-dependent case. The following equations express the stress and displacement field for this case, respectively:

$$\sigma_{22} = \frac{\sigma_{\infty}^{R}\, x}{\sqrt{x^2-a^2}} - \frac{p(t)\, x}{\sqrt{x^2-a^2}} + \frac{2p(t)x}{\pi\sqrt{x^2-a^2}}\, arcsin\left(\frac{a-\beta}{a}\right) - \frac{2p(t)}{\pi}\, arctan\left(\frac{(a-\beta)\sqrt{x^2-a^2}}{x\sqrt{2a\beta-\beta^2}}\right) \tag{107}$$

$$u_2 = \sigma_{\infty}^{R}\frac{k+1}{4G}\sqrt{a^2-x^2} - p(t)\frac{k+1}{4G}\sqrt{a^2-x^2} + \frac{k+1}{4G}\frac{2p(t)}{\pi}\Big(arcsin(c)\sqrt{a^2-x^2} - x \times$$
$$arctan\left(\frac{c}{\sqrt{1-c^2}}\frac{\sqrt{a^2-x^2}}{x}\right) + ac \times arctan\left(\frac{1}{\sqrt{1-c^2}}\frac{\sqrt{a^2-x^2}}{a}\right)\Big) \tag{108}$$

The stress and displacement field equations are written in dimensionless format as follows:

$$\frac{\sigma_{22}}{\sigma_{\infty}^{R}} = \frac{1}{\sqrt{1-\left(\frac{\mathrm{a}}{\mathrm{x}}\right)^2}} - \frac{p(t)}{\sigma_{\infty}^{R}}\frac{1}{\sqrt{1-\left(\frac{\mathrm{a}}{\mathrm{x}}\right)^2}} + \frac{2}{\pi}\frac{p(t)}{\sigma_{\infty}^{R}}\left(\frac{1}{\sqrt{1-\left(\frac{\mathrm{a}}{\mathrm{x}}\right)^2}}arcsin(c) - arctan\left(\frac{c\sqrt{1-\left(\frac{\mathrm{a}}{\mathrm{x}}\right)^2}}{\sqrt{1-(\mathrm{c})^2}}\right)\right) \tag{109}$$

$$\frac{u_2}{\frac{k+1}{4G}a\sigma_{\infty}^{R}} = \sqrt{1-\left(\frac{\mathrm{x}}{\mathrm{a}}\right)^2} - \frac{p(t)}{\sigma_{\infty}^{R}}\sqrt{1-\left(\frac{\mathrm{x}}{\mathrm{a}}\right)^2} + \frac{2}{\pi}\frac{p(t)}{\sigma_{\infty}^{R}}\Bigg(arcsin(c)\sqrt{1-\left(\frac{\mathrm{x}}{\mathrm{a}}\right)^2} - \frac{x}{a} \times$$
$$arctan\left(\frac{c}{\sqrt{1-\mathrm{c}^2}}\frac{\sqrt{1-\left(\frac{\mathrm{x}}{\mathrm{a}}\right)^2}}{\frac{x}{a}}\right) + c \times arctan\left(\frac{1}{\sqrt{1-\mathrm{c}^2}}\sqrt{1-\left(\frac{\mathrm{x}}{\mathrm{a}}\right)^2}\right)\Bigg) \tag{110}$$

The effects of both instantaneous healing and time-dependent bonding strength are considered in this study. As mentioned in the section 2.8, development of the mechanical property is dependent on the diffusion stage. Also, the fracture stress in diffusion stage is the sum of the stress due to wetting σ_0 and the stress due to diffusing σ_d. Wool and O'Connor (1981) stated that the diffusion of chain ends at some time of healing process may be delayed or prevented as a result

of chemical reaction and rearrangement of surface. Therefore, in order to solve this problem, a diffusion initiation function $\dot{\psi}(t)$ such that σ_d is obtained as:

$$\sigma_d = k' t^{0.25} * \dot{\psi}(t) \tag{111}$$

When the required chain ends are present for immediate reptation across the interface, then $\dot{\psi}(t) = \delta(t)$, and

$$\sigma_d = k' t^{0.25} \tag{112}$$

Also,

$$\sigma_b = \sigma_0 + k' t^{0.25} \tag{113}$$

Eq. (80) is in substituting $p(t)$ instead of using Eq. (113). Also, the instantaneous bonding strength or the initial bonding strength (σ_0) is considered to be equal $0.3\ \sigma_b(t_\infty)$ (Bhasin et al., 2008).

Therefore, the time-dependent bonding strength is expressed as follows:

$$\sigma_b(t) = 0.3\ \sigma_b(t_\infty) + (\sigma_b(t_\infty) - \sigma_0)\left(\frac{t}{t_\infty}\right)^{0.25} \tag{114}$$

Figure 29 demonstrates the influence of time-dependent bonding strength on normalized displacement. As it can be seen, NU value decreases due to an increase in the time period. A comparison of Figure 29(a), (b), and (c) indicates that NU decreases as a result of increases on ultimate bonding strength. In Figure 30, the impact of several healing process zone values on normalized displacement are presented. The greater healing process zone results in a reduction in displacement value.

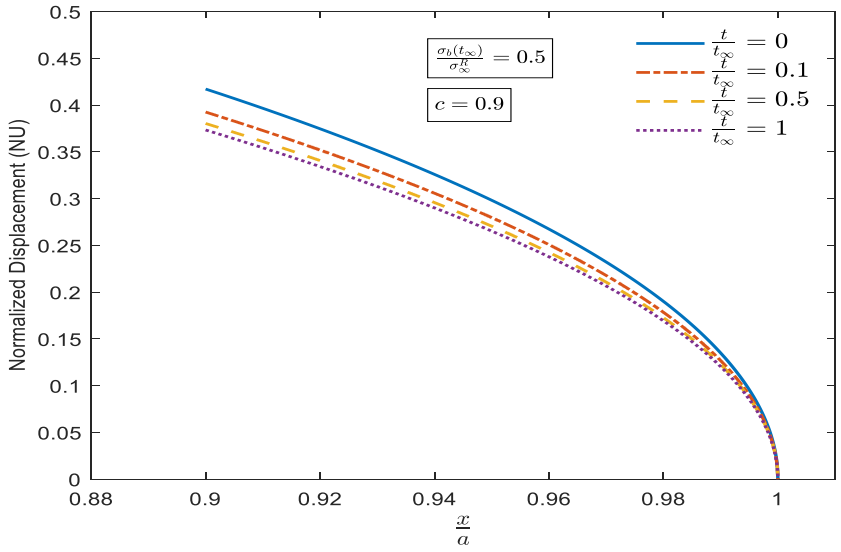

(a)

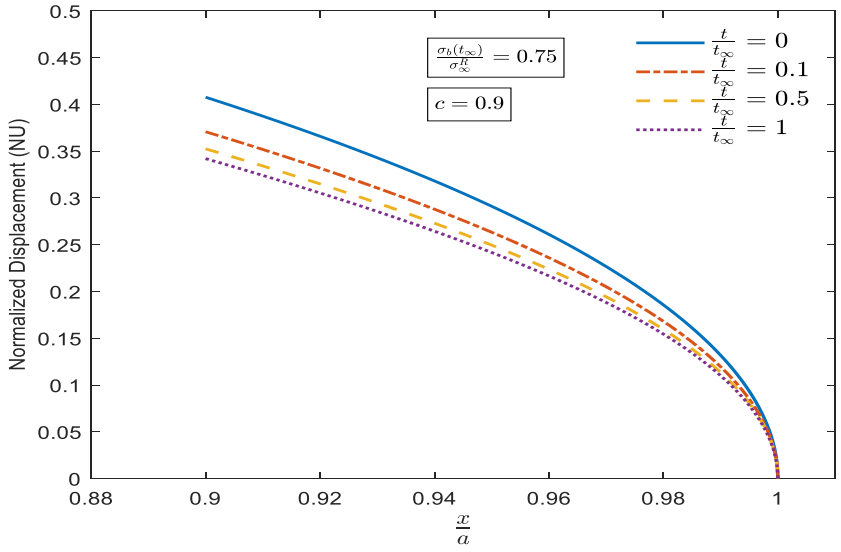

(b)

Figure 29 Normalized displacement under constant value of c and variable $\frac{\sigma_b(t_\infty)}{\sigma_\infty^R}$ in the case of time-dependent bonding strength.

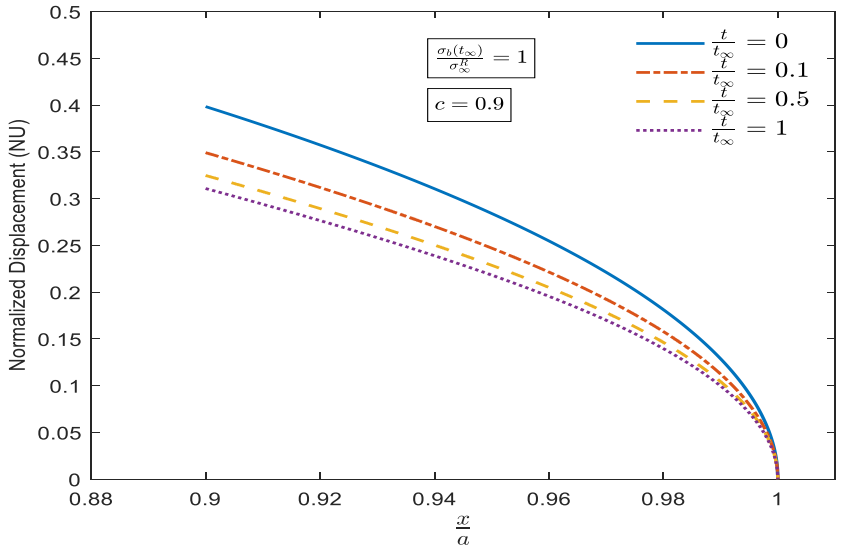

(c)

Figure 29 Continued.

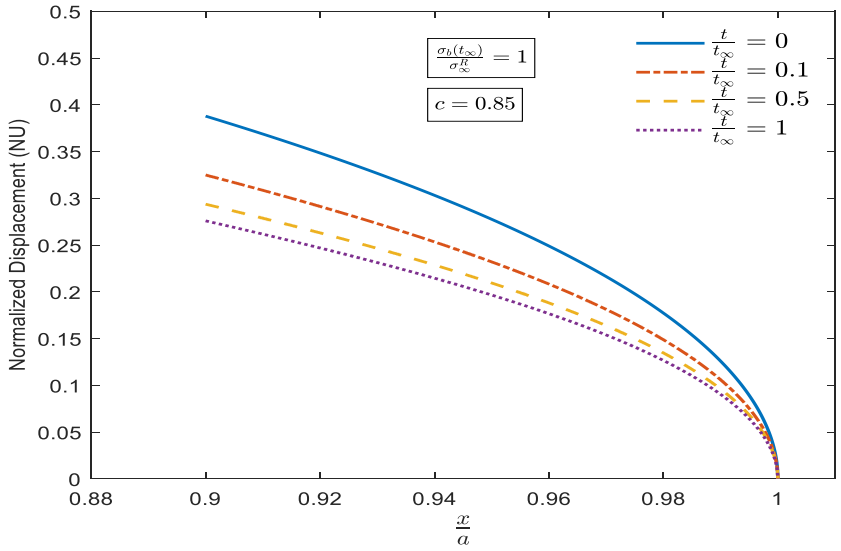

(a)

Figure 30 Normalized displacement under constant value of $\frac{\sigma_b(t_\infty)}{\sigma_\infty^R}$ and variable c in the case of time-dependent bonding strength.

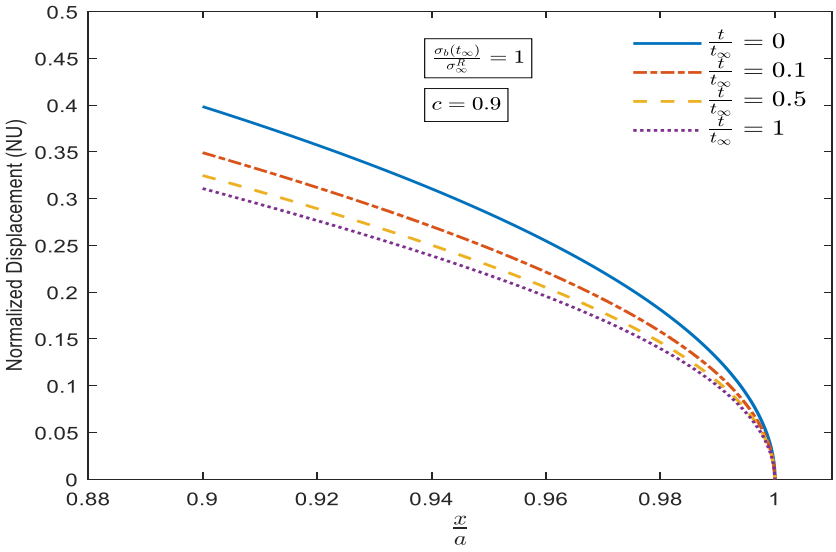

(b)

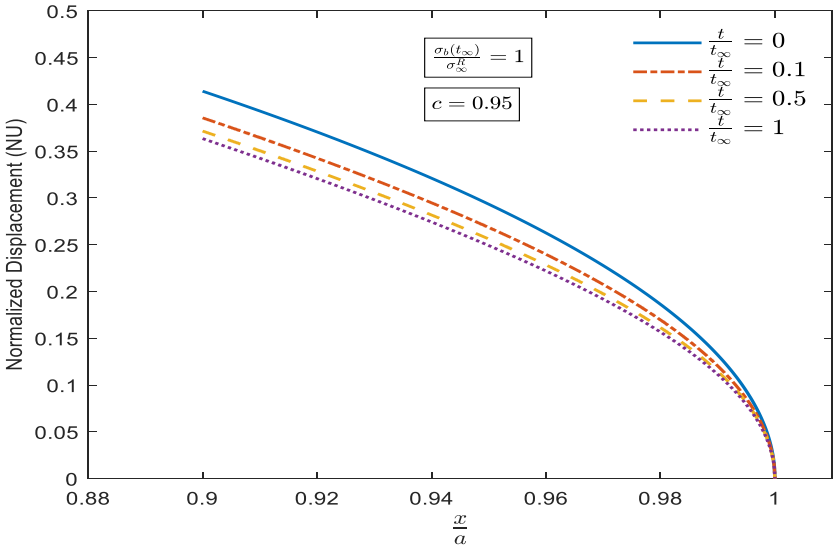

(c)

Figure 30 Continued.

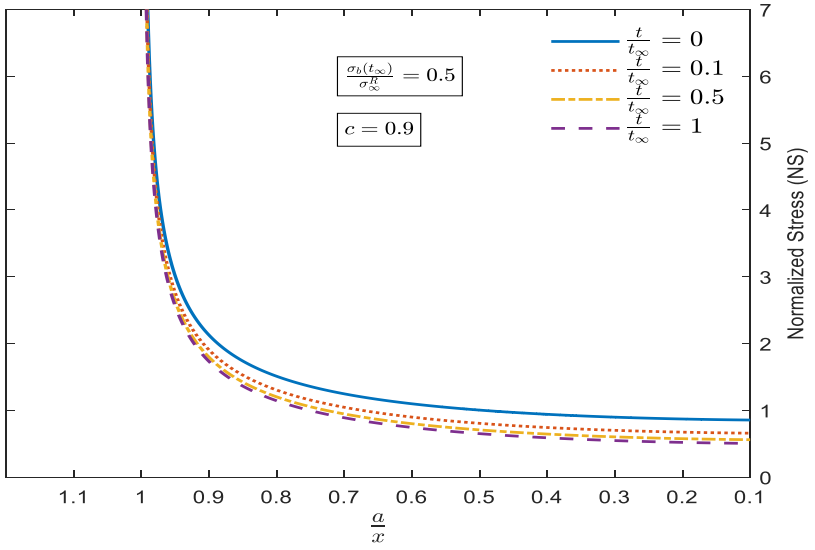

(a)

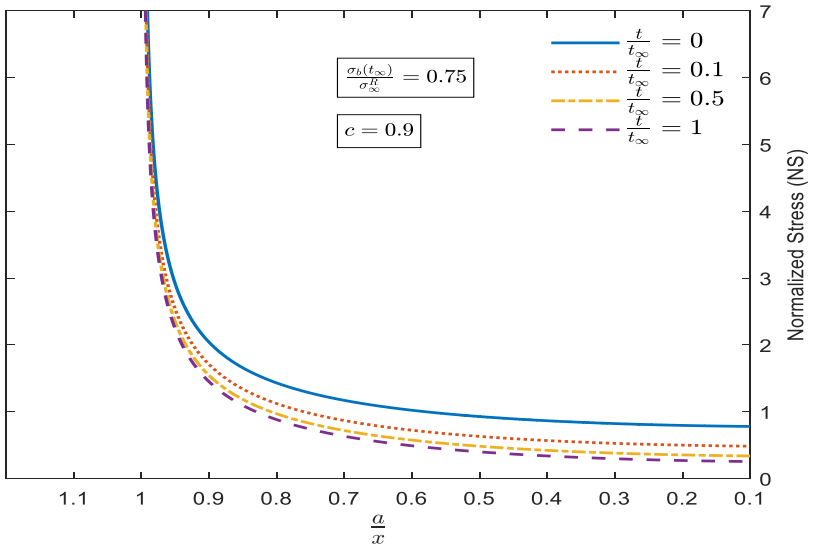

(b)

Figure 31 Normalized stress under constant value of c and variable $\frac{\sigma_b(t_\infty)}{\sigma_\infty^R}$ in the case of time-dependent bonding strength.

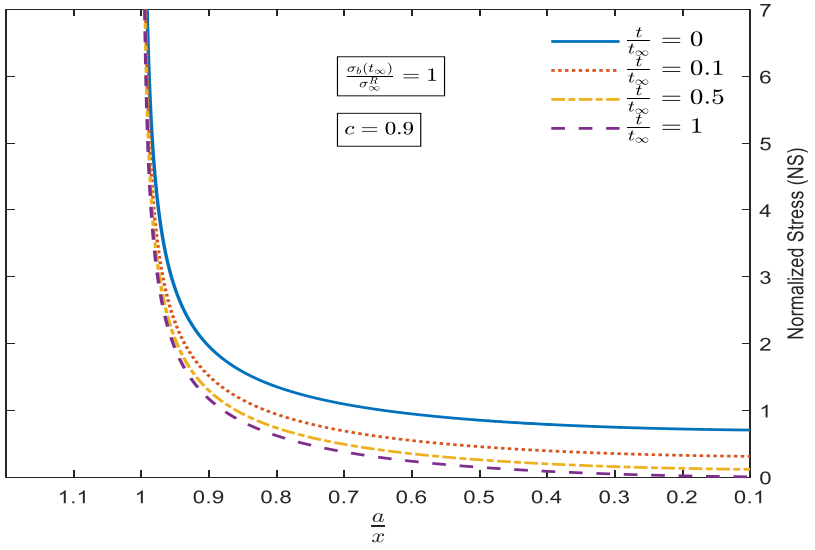

(c)

Figure 31 Continued.

Figure 32 demonstrates the effect of time-dependent bonding strength on the normalized stress. It is notable that as time passes, the increasing bonding strength decreases the NS value. Also, the NS decreases as the ultimate value of bonding strength increases. Furthermore, the influence of the healing process zone on the NS is shown in Figure 32. As it can be seen, a larger healing process zone has a greater effect on the reduction of NS value.

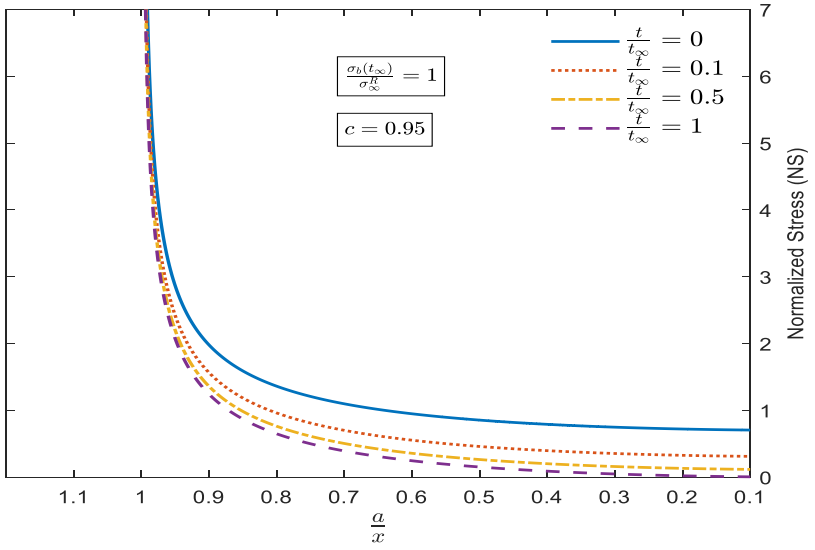

(a)

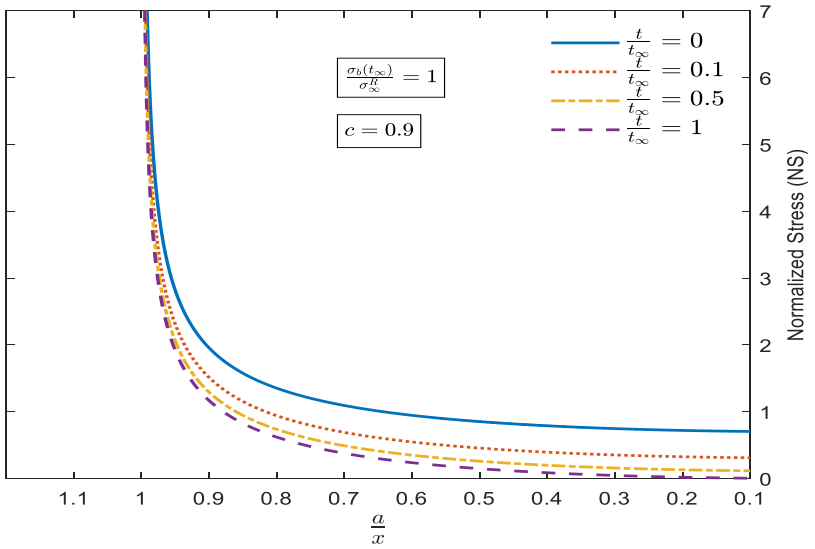

(b)

Figure 32 Normalized stress under constant value of $\frac{\sigma_b(t_\infty)}{\sigma_\infty^R}$ and variable c in the case of time-dependent bonding strength.

4.3 Stress and Displacement Fields in Viscoelastic Media

Time-independent bonding strength is an easy condition to defend. Assume the constant value for bonding strength can be solved, but this assumption (time-independent bonding strength) does not represent the true nature of the healing process. Therefore, the results of stress and displacement fields in elastic media are transformed into viscoelastic media using the correspondence principles in order to capture the actual response of the materials that have time-dependent properties. Using the third correspondence principle (CP-III), which is appropriate in analyzing the healing phenomenon (crack shortening), the value of the displacement field in viscoelastic media is the same as the value of the displacement field in elastic media. The displacement field in viscoelastic media is expressed as:

$$u_2 = \sigma_\infty^R \frac{k+1}{4G}\sqrt{a^2-x^2} - (\sigma_0 + k't^m)\frac{k+1}{4G}\sqrt{a^2-x^2} + \frac{k+1}{4G}\frac{2(\sigma_0+k't^m)}{\pi}\left(arcsin(c)\sqrt{a^2-x^2} - x^* arctan\left(\frac{c}{\sqrt{1-c^2}}\frac{\sqrt{a^2-x^2}}{x}\right) + ac^* arctan\left(\frac{1}{\sqrt{1-c^2}}\frac{\sqrt{a^2-x^2}}{a}\right)\right) \quad (115)$$

On the other hand, using the convolution integral, the bonding strength in the viscoelastic media begins to relax, which counters the increasing nature of bonding strength over time. Furthermore, Schapery (1989) assumed that bonding strength σ_b^{VE} is independent of time. He considered only instantaneous healing and assumed it as the total bond strength. The model used in this research combined the effects of both instantaneous healing and time-dependent bond strength. The work of Wool and O'Conner (1981) for modeling the long-term effect of healing is used in this model in order to capture the effects of both terms. So, computations begin with time-dependent bonding strength in elastic media instead of constant bonding strength.

Also, the impact of healing exponent m and λ on the stress field is evaluated. The following general formulation is used for bonding strength instead of using Eq. (113):

$$\sigma_b^R(t) = \sigma_0 + k't^m \tag{116}$$

where $0 < m < 1$. In this study, several values are chosen for m. Also, two distinctive values $(0.005 \text{ and } 0.05)$ are selected for λ in the relaxation modulus given by:

$$E(t) = E_\infty + (E_0 - E_\infty)e^{-\lambda t} \tag{117}$$

where $\lambda = \frac{1}{T_r}$ in which T_r is the relaxation time (Zhang and Greenfield, 2007).

To calculate the stress field in viscoelastic media, the following equations are used:

$$\sigma_b^{VE} = \{Ed\sigma_b^R\} = \frac{1}{E_R}\int_{0^-}^{t} E(t-\tau)\frac{d\sigma_b^R}{d\tau}d\tau \tag{118}$$

$$E(t) = E_\infty + (E_0 - E_\infty)e^{-\lambda t} \tag{119}$$

$$\sigma_b^R(t) = \sigma_0 + k't^m \tag{120}$$

Substituting into Eq. (118)

$$\sigma_b^{VE} = E(t)\frac{1}{E_R}\sigma_0 + \frac{1}{E_R}E_\infty k't^m + e^{-\lambda t}\int_{0^-}^{t}\frac{E_0 - E_\infty}{E_R}e^{\lambda\tau}mk'\tau^{m-1}\,d\tau \tag{121}$$

Evaluating this integral yield:

$$\sigma_b^{VE} = E(t)\frac{1}{E_R}\sigma_0 + \frac{1}{E_R}E_\infty k't^m + \frac{E_0 - E_\infty}{E_R}k'me^{-\lambda t}\frac{\Gamma(m) - \Gamma(m,-\lambda t)}{(-\lambda)^m} \tag{122}$$

The three terms in Eq. (122) show: first, a relaxation in instantaneous healing; second, an enlargement in the value of bonding strength as a result of time-dependent bonding stress which reaches an asymptotic value of $\frac{1}{E_R}E_\infty k't^m$; third, the coupling effect of recovery and relaxation. To simplify, $P\sigma 3$ defines the value of part of the third term $\left(me^{-\lambda t}\frac{\Gamma(m)-\Gamma(m,-\lambda t)}{(-\lambda)^m}\right)$. The value of $P\sigma 3$ will ultimately reach zero if enough time is given to the material with a long relaxation time.

As it can be seen in Figure 33, the bonding strength increases as the value of m increases. Also, an increase in the value of λ is a decrease in the value of relaxation time which has a negative impact on $P\sigma 3$ reducing the time of the peak value of $P\sigma 3$.

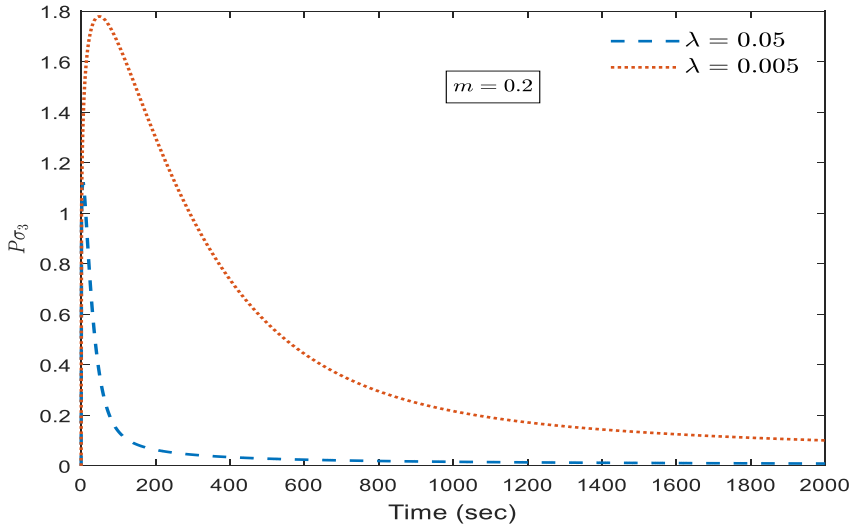

(a)

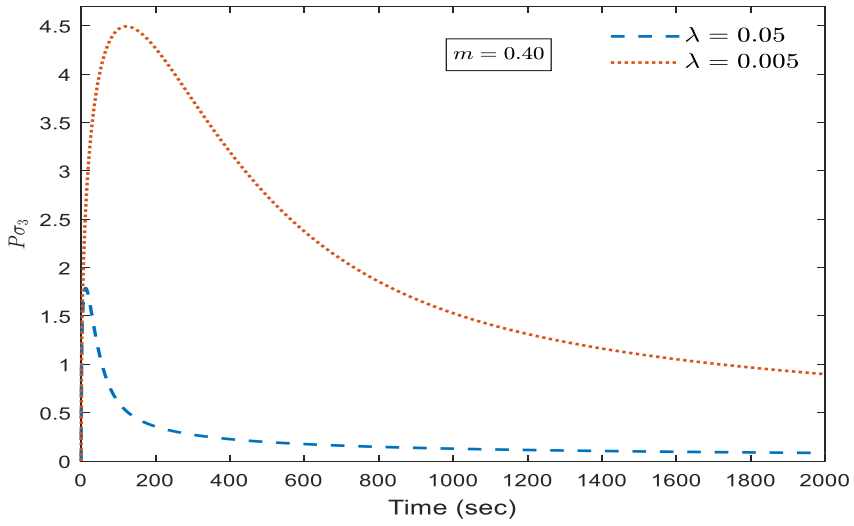

(b)

Figure 33 Influence of distinctive value of healing exponent m on $P\sigma 3$.

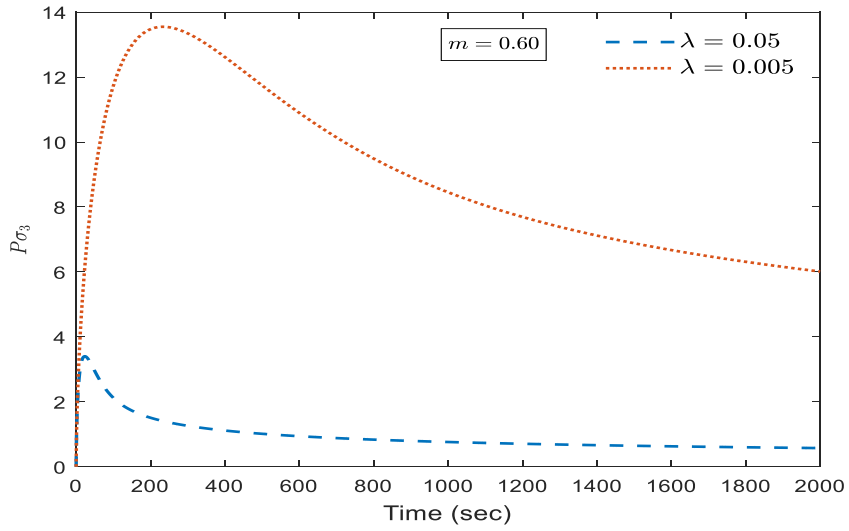

(c)

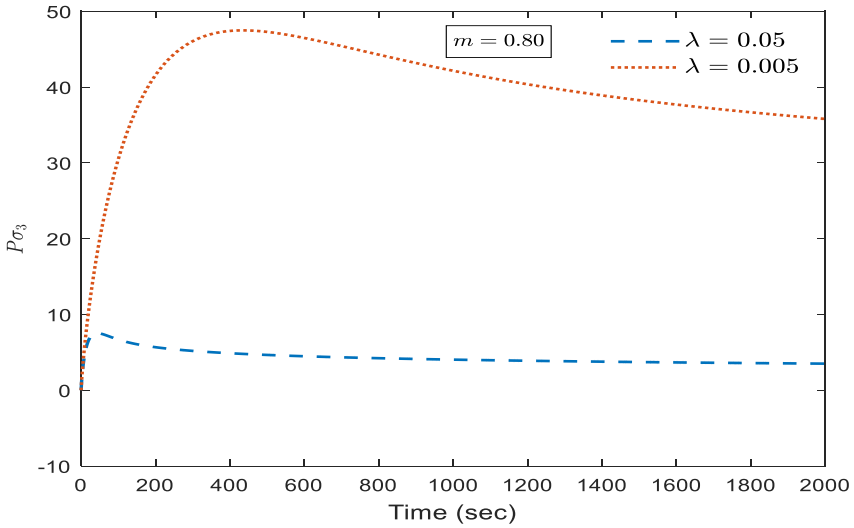

(d)

Figure 33 Continued.

Since λ is time and temperature dependent, the relaxation process increases at high temperature. Consequently, as the relaxation time decreases, it causes an increase in value of λ. The effect of different bonding strength coefficients with a constant relaxation time is shown in

Figure 34. The stress field near the crack tip increases as a result of an increase in the value of bond strength.

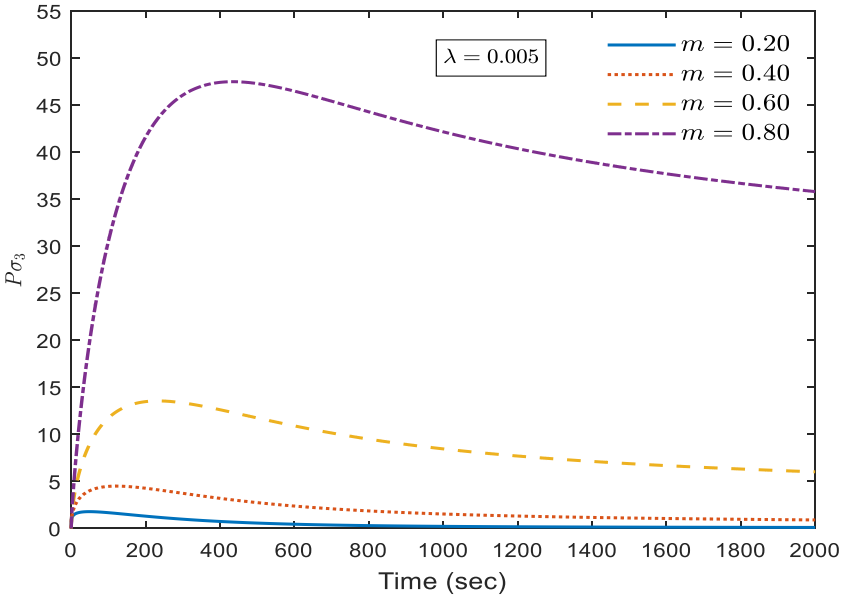

(a)

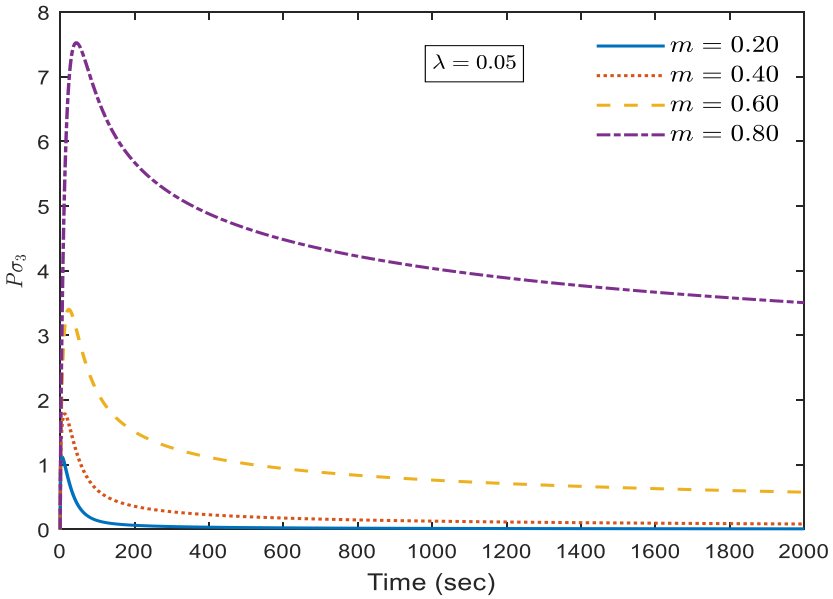

(b)

Figure 34 Influence of distinctive value of λ on $P\sigma 3$.

5. CONCLUSIONS AND RECOMMENDATIONS FOR FUTURE STUDY

5.1 Conclusion

The influence of microdamage healing on stress intensity factor (SIF), displacement, and stress fields near a crack tip in the materials that have the capability to heal is investigated. The microdamage healing model that is used in this study considers the effects of both instantaneous healing (short-term) and time-dependent bonding strength (long-term). The influence of microdamage healing on crack propagation is examined in elastic media by using analytical relations for SIF and by considering the healing process. Also, the effects of healing of microdamage on the displacement field and stress field in proximity to a crack tip in elastic media are investigated using multiple conditions. For instance, the impact of loading and loading condition is considered since pavement structure is not under constant load. Furthermore, the results of stress and displacement fields in elastic media are translated into viscoelastic media using the third correspondence principle (CP-III) in order to capture the actual response of the materials that have time-dependent properties. Finally, the effect of using distinctive coefficients in defining the strength of bonding and relaxation time are evaluated.

Based on the findings of this research, the following conclusions were drawn:

- The rest periods have an effect on both bonding strength and bonding zone length (healing process zone). Longer rest periods lead to a larger healing process zone and greater bonding strength value.
- The forces between the crack surfaces attempt to reduce the distance between the crack surfaces and close the opening, and as a result, an increase in the bonding strength causes a decrease in the SIF.

- The far field stress must be greater when the effect of healing is considered in order to propagate the crack and to reach a specific crack opening.
- The stress and displacement fields proximal to the crack tip decrease as a result of an increase in the value of bond strength.
- The bonding strength increases as the healing exponent m value increases.
- The relaxation process increases at high temperature. Consequently, the relaxation time decreases, which results in an increase in value of λ.

5.2 Future Study

The current study is part of a larger project that aims to develop a sophisticated model to predict the effect of microdamage healing on bituminous material. Therefore, the following tasks need to be accomplished in order to achieve this goal.

1. Derive analytical relations for energy release rate G by considering the healing process to capture the actual response of the materials that have time-dependent properties.
2. Quantify the work done by the crack surfaces.
3. Perform finite element analysis in order to predict the accuracy of the model.
4. Determine a test procedure to validate the model.

REFERENCES

Bhasin, A., Little, D.N., Bommavaram, R., Vasconcelos, K., 2008. A framework to quantify the effect of healing in bituminous materials using material properties. Road Materials and Pavement Design 9, 219-242.

Bhasin, A., Bommavaram, R., Greenfield, M.L., Little, D.N., 2011. Use of molecular dynamics to investigate self-healing mechanisms in asphalt binders. Journal of Materials in Civil Engineering (ASCE) 23, 485-492.

Bommavaram, R.R., Bhasin, A., Little, D.N., 2009. Determining intrinsic healing properties of asphalt binders. Transportation Research Record: Journal of the Transportation Research Board 2126, 47-54.

Bonnaure, F. P., Huibers, A. H. J. J., Boonders, A., 1982. A laboratory investigation of the influence of rest periods on the fatigue characteristics of bituminous mixes. Journal of the Association of Asphalt Paving Technologists 51, 104-128.

Broek, D., 1986. Elementary engineering fracture mechanics. Kluwer Academic Publishers Group, Netherlands.

Brown, E.N., Sottos, N.R., White, S.R., 2002. Fracture testing of a self-healing polymer composite. Experimental Mechanics 42, 372-379.

Carpenter, S.H., Ghuzlan, K., Shen, S., 2003. Fatigue endurance limit for highway and airport pavements. Transportation Research Record, 131-138.

Carpenter, S.H., Shen, S., 2006. A dissipated energy approach to study HMA healing in fatigue. 85th Annual Meeting of the Transportation Research Board Washington DC.

De Gennes, P.G., 1971. Reptation of a polymer chain in the presence of fixed obstacles. The Journal of Chemical Physics 55, 572-579.

Elber, W., 1970. Engineering Fracture mechanics 71, 37.

Elber, W., 1971.The significance of fatigue crack closure. Damage tolerance in aircraft structures. American Society for Testing and Materials, 230-242.

Elphingstone, G.M., 1997. Adhesion and cohesion in asphalt-aggregate systems. Ph.D. Dissertation, Texas A&M University, College Station, Texas.

Findley, W.N., Lai, J.S., Onaran, K., 1989. Creep and relaxation of nonlinear viscoelastic materials: with an introduction to linear viscoelasticity. Dover Publications, United States.

Griffith, A.A., 1921. The phenomena of rupture and flow in solids. Philosophical Transactions of the Royal Society of London. Series A, Containing Papers of a Mathematical or Physical Character 221, 163-198.

Groenendijk, J., 1998. Accelerated testing and surface cracking of asphalt concrete pavements. Delft University of Technology.

Inglis, C.E., 1913. Stresses in a plate due to the presence of cracks and sharp corners. Transactions of the Institution of Naval Architects 55, 219-241.

Irwin, G.R., 1957. Analysis of stresses and strains near the end of a crack traversing a plate. Journal of Applied Mechanics 24, 361-364.

Kessler, M.R., White, S.R., 2001. Self-activated healing of delamination damage in woven composites. Composites Part a-Applied Science and Manufacturing 32, 683-699.

Kim, Y.H., Wool, R.P., 1983. A theory of healing at a polymer-polymer interface. Macromolecules 16, 1115-1120.

Kim, Y.R., Little, D.N., 1990. One-dimensional constitutive modeling of asphalt concrete. Journal of Engineering Mechanics (ASCE) 116, 751-772.

Kim, Y.R., Little, D.N., Benson, F.C., 1990. Chemical and mechanical evaluation on healing mechanism of asphalt concrete (with discussion). Journal of the Association of Asphalt Paving Technologists 59, 240-275.

Kim, Y. R., Lee, H. J., and Little, D. N., 1997. Fatigue characterization of asphalt concrete using viscoelasticity and continuum damage theory. Journal of the Association of Asphalt Paving Technologists 66, 520-569.

Kim, Y.R., Little, D.N., Lytton, R.L., 2001. Evaluation of microdamage, healing, and heat dissipation of asphalt mixtures, using a dynamic mechanical analyzer. Transportation Research Record: Journal of the Transportation Research Board 1767, 60-66.

Kim, Y., Little, D.N., and Lytton, R.L., 2002. Use of dynamic mechanical analysis (DMA) to evaluate the fatigue and healing potential of asphalt binders in sand asphalt mixtures. Journal of the Association of Asphalt Paving Technologists 71,176-206.

Kim, Y.R., 2003. Fatigue and healing characterization of asphalt mixtures. Journal of Materials in Civil Engineering 15, 75-83.

Kim, B., and Roque, R., 2006. Evaluation of healing property of asphalt mixture. Proc., 85th Annual Meeting of the Transportation Research Board, Washington, DC.

Lee, H.J., Kim, Y.R., 1998. Viscoelastic continuum damage model of asphalt concrete with healing. Journal of Engineering Mechanics (ASCE) 124, 1224-1232.

Little, D. N., Lytton, R. L., Williams, D., and Kim, Y. R., 1997. Propagation and healing of micro-cracks in asphalt concrete and their contributions to fatigue. In Asphalt Science and Technology, 149-195.

Little, D. N., Lytton, R. L., Williams, D., and Kim, Y. R., 1999. An analysis of the mechanism of microdamage healing based on the application of micromechanics first principles of fracture and healing. Journal of the Association of Asphalt Paving Technologists 42, 501-542.

Little, D.N., Lytton, R., Williams, D., Chen, C., 2001. Microdamage healing in asphalt and asphalt concrete, Volume I: Microdamage and microdamage healing, Project summary report.

Little, D.N., Bhasin, A., 2007. Exploring mechanism of healing in asphalt mixtures and quantifying its impact. Springer Series in Materials Science 100, 205-218.

Lytton, R. L., Uzan, J., Fernando, E. G., Roque, R., Hiltunen, D. R., and Stoffels, S. M., 1993. Development and validation of performance prediction models and specifications for asphalt binders and paving mixes. Rep. No. SHRP-A-357, Strategic Highway Research Program, National Research Council, Washington, DC. 26.

Lytton, R. L., Little, D. N. et al., 1997. Propagation and healing of micro-cracks and their contributions to fatigue. Asphalt Science and Technology, 149-195.

Lytton, R. L., Chen, J. C. W., and Little, D. N., 1998. Fundamental properties of asphalt and modified asphalts-Task K-Microdamage healing in asphalt and asphalt concrete. In Continuum Damage Mechanics and Micromechanics Model to Explain Fatigue Damage and Microcrack Healing in Asphalt Mixtures, Final Report, FHWA, U.S. Department of Transportation. Vol.3. 28.

Lytton, R. L., 2000. Characterizing asphalt pavements for performance. Transportation Research Record, 5-16.

Mahsa, A., 2013. Modeling micro-damage healing mechanism at micro-scale. Master Thesis, Texas A&M University, College Station, Texas.

Maillard S, De La Roche C, Hammoum F, Gaillet L, and Such C, 2004. Experimental investigation of fracture and healing of bitumen at pseudo contact of two aggregates. 3rd Eurasphalt & Eurobitume Congress, 266.

Mueller, H., 1971. Stress-intensity factor and crack opening for a linearly viscoelastic strip with a slowly propagating central crack. International Journal of Fracture Mechanics 7, 129-141.

Prager, S., Tirrell, M. J., 1981.The healing process at polymer-polymer interfaces. The Journal of Chemical 75, 5194-5198.

Reinhardt, H.W., Jooss, M., 2003. Permeability and self-healing of cracked concrete as a function of temperature and crack width. Cement and Concrete Research 33, 981-985.

Schapery, R.A., 1984. Correspondence principles and a generalized j integral for large deformation and fracture-analysis of viscoelastic media. International Journal of Fracture 25, 195-223.

Schapery, R.A., 1989. On the mechanics of crack closing and bonding in linear viscoelastic media. International Journal of Fracture 39, 163-189.

Shell. Shell pavement design manual -asphalt pavement and overlays for road traffic. London, UK: Shell International Petroleum Company Limited; 1978.

Sedov, L., 1972. A course in continuum mechanics. Volume 4- Elastic and plastic solids and the formation of cracks (Book- A course in continuum mechanics. Volume 4- Elastic and plastic solids and the formation of cracks.). Groningen, Wolters-Noordhoff Publishing, 1972. 325.

Shen, S., Carpenter, S.H., 2007. Development of an asphalt fatigue model based on energy principles. Journal of Assoc. Asphalt Paving. Technol76, 525-74.

Shen, S., Chiu, H.M., Huang, H., 2010. Characterization of fatigue and healing in asphalt binders. Journal of Materials in Civil Engineering 22, 846.

Tan, Y., Shan, L., Richard Kim, Y., Underwood, B.S., 2012. Healing characteristics of asphalt binder. Construction and Building Materials 27, 570-577.

Westergaard, H.M., 1934.Stresses at a crack, size of the crack and the bending of reinforced concrete. Proceedings of the American Concrete Institute 30, 93-102.

Westergaard, H.M., 1939. Bearing pressure and cracks. Journal of Applied Mechanics 6, 49-53.

Williams, M., 1957. On the stress distribution at the base of a stationary crack. Journal of Applied Mechanics 24, 109-114.

Williams, M., 1959. The stresses around a fault or crack in dissimilar media. Bulletin of the Seismological Society of America 49, 199-204.

Williams, D., Little, D., Lytton, R., Kim, Y., Kim, Y., 2001. Microdamage healing in asphalt and asphalt concrete, volume II: laboratory and field testing to assess and evaluate microdamage and microdamage healing.

Wool, R., O'Connor, K.M., 1981. A theory of crack healing in polymers. Journal of Applied Physics 52, 5953-5963.

Wool, R., O'Connor, K.M, 1982. Time dependence of crack healing. Journal of Polymer Science: Polymer Letters Edition 20, 7-16.

Zhang, L., Greenfield, M.L., 2007. Relaxation time, diffusion, and viscosity analysis of model asphalt systems using molecular simulation. The Journal of Chemical Physics 127, 194502.